Colloquium: Quantum matter built from nanoscopic lattices of atoms and photons

D. E. Chang

ICFO-Institut de Ciències Fotòniques, The Barcelona Institute of Science and Technology, Mediterranean Technology Park, 08860 Castelldefels, Barcelona, Spain and ICREA-Institució Catalana de Recerca i Estudis Avançats, 08015 Barcelona, Spain

J. S. Douglas

ICFO-Institut de Ciències Fotòniques, The Barcelona Institute of Science and Technology, Mediterranean Technology Park, 08860 Castelldefels, Barcelona, Spain

A. González-Tudela

Max-Planck-Institut für Quantenoptik Hans-Kopfermann-Strasse 1, 85748 Garching, Germany

C.-L. Hung

Department of Physics and Astronomy, and Purdue Quantum Center, Purdue University, West Lafayette, Indiana 47907, USA

H. J. Kimble

Norman Bridge Laboratory of Physics 12-33, California Institute of Technology, Pasadena, California 91125, USA

(published 1 August 2018)

This Colloquium describes a new paradigm for creating strong quantum interactions of light and matter by way of single atoms and photons in nanoscopic lattices. Beyond the possibilities for quantitative improvements for familiar phenomena in atomic physics and quantum optics, there is a growing research community that is exploring novel quantum phases and phenomena that arise from atom-photon interactions in one- and two-dimensional nanophotonic lattices. Nanophotonic structures offer the intriguing possibility to control atom-photon interactions by engineering the medium properties through which they interact. An important aspect of these new research lines is that they have become possible only by pushing the state-of-the-art capabilities in nanophotonic device fabrication and by the integration of these capabilities into the realm of ultracold atoms. This Colloquium attempts to inform a broad physics community of the emerging opportunities in this new field on both theoretical and experimental fronts. The research is inherently multidisciplinary, spanning the fields of nanophotonics, atomic physics, quantum optics, and condensed matter physics.

DOI: 10.1103/RevModPhys.90.031002

CONTENTS

I. Introduction 2
II. Conventional Strong Atom-photon Interactions 3
III. A New Way Forward: Atoms and Nanophotonics 5
  A. Overview of nanophotonics 5
  B. Optical nanofibers 7
  C. 1D and 2D photonic crystal waveguides 7
  D. Nanophotonic optical cavities 8
  E. Imperfections 9
IV. A Surprising Future for Atom-photon Physics 10
  A. Quantum coherence in a strongly dissipative regime 10
  B. Chiral quantum optics 11
  C. Quantum many-body physics for atomic spins in a band gap 12
  D. Coupled cavity arrays 13
V. Atom-light Interactions in Dielectrics: A Green's-function-based Approach 13
VI. Atom Trapping Within Dielectric Nanostructures 14
  A. Overview of optical traps for nanophotonics 14
  B. Casimir-Polder potentials 16
  C. 2D vacuum lattices 17
VII. Collective Dissipation 17
  A. Effective description 17
  B. Dynamics within decoherence-free subspaces 18
VIII. Spin-orbit Coupling of Light 19
  A. Effective description for a chiral setup 19
  B. Nonreciprocal photon transport 20
  C. Many-body entangled steady states 20

IX. Band-gap Physics 20
A. Designing band-gap interactions with the atomic physics toolbox 21
1. Dynamically shaping interactions with Raman lasers 22
2. Full control of spin interactions 22
B. Perspective: Multiphysics coupling 23
X. Spins and Motion: Semiclassical and Quantum Self-organization 23
XI. Quantum Dielectrics: Photon-photon Interactions 24
XII. Outlook 26
Acknowledgments 26
References 27

I. INTRODUCTION

Achieving and controlling interactions between atoms and photons at the quantum level has been a central goal in the fields of atomic physics and quantum optics for decades. Atomic systems have long provided a platform to observe many fundamental quantum phenomena, such as nonclassical statistics of light emitted by single atoms (Kimble, Dagenais, and Mandel, 1977) and reversible vacuum Rabi oscillations between a single atom and a photon (Rempe, Walther, and Klein, 1987; Thompson, Rempe, and Kimble, 1992; Brune *et al.*, 1996). Such early examples of the capability to observe and generate quantum effects gained new importance with the rise of fields such as quantum information processing and quantum metrology, making already well-studied atom-light interfaces a promising route toward realization. There have been spectacular demonstrations as diverse as single-photon switching (O'Shea *et al.*, 2013; Shomroni *et al.*, 2014) and basic quantum networks (Ritter *et al.*, 2012) using atoms coupled to high-finesse optical cavities, and quantum memories for light (Liu *et al.*, 2001; Phillips *et al.*, 2001; Julsgaard *et al.*, 2004; Chou *et al.*, 2007) and entanglement-enhanced magnetometry using atomic ensembles (Wasilewski *et al.*, 2010). Beyond these applications, the combination of complex interactions that can occur in atom-light interfaces and the level of experimental control that can be reached also makes these systems promising to investigate new types of many-body phenomena and opens up interesting links with fields such as quantum information theory and condensed matter. Active areas of interest along these lines include self-organization of atoms due to the interplay between atomic scattering of light and optical forces (Domokos and Ritsch, 2002; Black, Chan, and Vuletic, 2003; Gopalakrishnan, Lev, and Goldbart, 2009; Baumann *et al.*, 2010), the behavior of strongly interacting photon "gases" (Peyronel *et al.*, 2012; Bienias *et al.*, 2014; Zeuthen *et al.*, 2017), and even the exploration of quantum information scrambling (Swingle *et al.*, 2016).

Historically, atom-light interfaces have consisted of macroscopic, free-space setups. Despite many experimental successes, there has also been an effort for over a decade to migrate from free space to microphotonic and nanophotonic platforms (Aoki *et al.*, 2006; Nayak *et al.*, 2007; Vetsch *et al.*, 2010; Volz *et al.*, 2011; Goban *et al.*, 2012, 2014; O'Shea *et al.*, 2013; Thompson *et al.*, 2013; Shomroni *et al.*, 2014) for a number of motivations. For example, the ability to confine light to small dimensions directly increases the per-photon field intensities and thus the interaction strengths with matter. At the same time, using photonic systems fabricated from state-of-the-art lithographic techniques provides a possible route toward robustness and scalability, perhaps even eventually leading to atomic physics and quantum optics on a chip. While experimental efforts began over a decade ago, success proved to be quite challenging. In particular, the nature of fields confined in nanophotonic systems, such as their polarization and dispersion relation, can be quite different than in free space. Thus, the large atomic physics toolbox built up for free-space atom loading, cooling, and trapping in general does not immediately apply when it comes to confining atoms within nanoscale regions of dielectric structures. The development of elegant schemes, such as traps formed from evanescent fields at two very different wavelengths or from light reflected from dielectric interfaces, was critical to experimental progress. Promisingly, important figures of merit for atom-light interactions, such as optical depth or a cavity "cooperativity" factor, are now competitive with or even exceed what is possible in free space (Tiecke *et al.*, 2014), representing a significant milestone for the field.

While the original motivation of migrating to nanophotonics largely centered on improving upon free-space approaches, the complexity of fields in nanophotonic systems also turns out to give rise to unanticipated opportunities. In particular, an increasing body of work demonstrates the possibility to create fundamentally new paradigms for quantum atom-light interactions, which have no obvious prior analog in free-space settings. This provides new routes toward building exotic quantum matter from atoms and photons, quantum simulation, and the transfer and manipulation of quantum information. For example, it has been shown that it is possible to realize chiral interactions between atoms and light, where atoms couple to photons (and thus to each other) in a directionally dependent way, even if the system is nominally mirror symmetric (Mitsch *et al.*, 2014; Sayrin, Junge *et al.*, 2015). It is also possible to realize atom-photon bound states, where an atom is surrounded by a localized photonic "cloud," and which can serve as a mediator of coherent long-range interactions between atoms.

Within this context, the goal of this Colloquium is to provide an overview of the progress, challenges, and new techniques involved in interfacing atomic physics and nanophotonics, and of the potential opportunities made possible by these emerging systems. We begin in Sec. II by reviewing the various approaches in free space to efficiently couple atoms and photons, which later will enable a better understanding of nanophotonics-based approaches. An overview of nanophotonic systems and the potential improvements in figures of merit over free space are discussed in Sec. III. In Sec. IV, we introduce the novel classes of paradigms that have emerged in recent years to control and manipulate atom-light interactions using nanophotonic systems, which can be roughly classified into three categories: the utilization of collective dissipation, chiral atom-light interactions, and interactions within a photonic "band gap." A more in-depth look is provided in the remainder of the Colloquium. In Sec. V, we introduce a theoretical formalism that enables one to conveniently capture atom-photon interactions in complex dielectric environments,

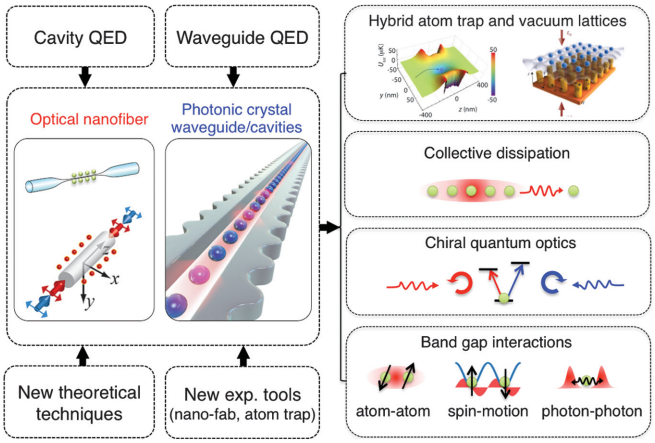

FIG. 1. Overview. Recent developments in experimental and theoretical techniques bring forth new atom-light interfaces (Sec. III) that can simultaneously achieve stable atom trapping and strong atom-photon interactions beyond conventional settings (Sec. II), and offer surprising new paradigms in atomic physics, cavity QED, and waveguide QED (Sec. IV). In this Colloquium we discuss these new possibilities, including a hybrid atom trap and vacuum lattices (Sec. VI), collective dissipation engineering (Sec. VII), chiral quantum optics (Sec. VIII), and many-body physics with atom-atom (Sec. IX), spin-motion (Sec. X), and photon-photon (Sec. XI) interactions.

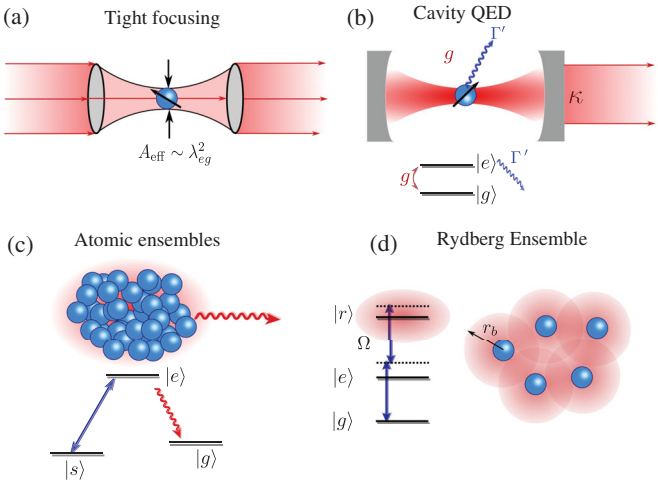

FIG. 2. Conventional approaches in quantum optics to achieve strong atom-photon interactions. (a) Diffraction-limited focusing of an optical beam onto a tightly trapped atom, (b) cavity QED, where the interaction is enhanced by a large number of photon round-trips, (c) atomic ensemble, where a large atom number results in high probability of interaction with a single photon, and (d) atomic ensemble of Rydberg atoms.

while in Sec. VI we describe different experimental techniques to create and load atomic traps near dielectric nanostructures. In the remaining sections, we return to the themes of collective dissipation, chiral interactions, and physics within a photonic band gap, introducing the minimal theoretical models that characterize each situation and providing simple examples of the applications and phenomena that emerge (see Fig. 1).

As a final note, while we specifically focus on work to interface neutral atoms with nanophotonic systems, many of the conceptual paradigms that emerge to control light-matter interactions can also be applied to other settings. These include molecules (Hwang *et al.*, 2009; Faez *et al.*, 2014), quantum dots and other solid-state emitters coupled to nanophotonic systems (Lodahl, Mahmoodian, and Stobbe, 2015), and superconducting qubits coupled to devices in the microwave domain (van Loo *et al.*, 2013; Liu and Houck, 2017). The general applicability of the paradigms presented here should become apparent (e.g., via the simple effective Hamiltonians governing them), while we refer readers to the references previously cited to learn the details of these other nonatomic systems.

II. CONVENTIONAL STRONG ATOM-PHOTON INTERACTIONS

Efficient interactions between atoms and light constitute the key enabling mechanism for applications with atomic systems, ranging from quantum information processing to metrology to nonlinear optics (Chang, Vuletic, and Lukin, 2014). We begin by reviewing several important concepts to achieve efficient interactions and highlighting some of the approaches used historically for atoms in free space.

The simplest model for an atom, which already elucidates the important physics, involves just two electronic levels, a ground state $|g\rangle$ and an excited state $|e\rangle$, which are connected through an optical dipole transition. The two-level nature implies that atoms can only emit and absorb single photons at a time, which has long been known to yield interesting nonlinear optical effects such as self-induced transparency (McCall and Hahn, 1969). Pioneering studies in fact showed that single-photon emission from an atom is intrinsically nonclassical, in both its intensity correlation statistics ("antibunching") (Kimble, Dagenais, and Mandel, 1977) and its photon number distributions (Short and Mandel, 1983). Together with nonclassical light from atomic ensembles (Freedman and Clauser, 1972; Clauser, 1974), these early experiments set the stage to make atomic systems one of the preferred avenues toward implementation of quantum information science.

One of the great incongruities, however, is that although single atoms *naturally* produce quantum states of light, getting a single atom and a photon to interact deterministically is very *unnatural*. An important parameter to characterize the interaction probability is the resonant scattering cross section σ_{sc} of a single atom [see Fig. 2(a)]. Here a weak incident laser beam, whose frequency is tuned to be resonant with the atomic transition ω_{eg} (with corresponding wavelength $\lambda_{eg} = 2\pi c/\omega_{eg}$), is focused with an area A_{eff} onto a single atom. The probability P that a photon in the beam is absorbed by the atom and rescattered into other directions in the paraxial approximation is $P = \sigma_{\text{sc}}/A_{\text{eff}}$. For an ideal two-level system, $\sigma_{\text{sc}} = 3\lambda_{eg}^2/2\pi$ is the maximum allowed by the unitarity limit and depends only on the transition wavelength of the atom but not its detailed microscopic properties (de Vries, van Coevorden, and Lagendijk, 1998). The difficulty of achieving a high probability of interaction lies in the fact that

in free space, the diffraction limit sets the lower limit of focusing to $A_{\mathrm{eff}} \gtrsim \lambda_{eg}^2$.

Given this fundamental observation, a number of approaches have been developed to increase P in free space (Chang, Vuletic, and Lukin, 2014).

(i) Tight focusing: Following the analysis of van Enk and Kimble (2001), pioneering efforts were made to tightly trap single atoms and to focus free-space beams onto them with high numerical aperture optics (Darquie *et al.*, 2005; Tey *et al.*, 2008; Hetet *et al.*, 2011), as shown in Fig. 2(a). It was observed that a single atom could attenuate the transmission of near-resonant light by up to $P \sim 10\%$.

(ii) Cavity QED: The predominant approach has been that of cavity quantum electrodynamics (QED), where single atoms are positioned within two mirrors that form a high-finesse optical cavity [Fig. 2(b)]. Here the probability of interaction is enhanced by the number of round-trips that the photon makes across the atom due to reflection off the mirrors. The resulting figure of merit $C \propto \sigma_{\mathrm{sc}} N_{\mathrm{trips}}/A_{\mathrm{eff}}$ of course loses its meaning as a probability of interaction when $C \gtrsim 1$, but as we show later, this cavity cooperativity factor defines a rather universal parameter to characterize the efficacy of a cavity QED system. It is also convenient to rewrite $N_{\mathrm{trips}} = c/\kappa L$ in terms of the cavity length L and decay rate κ, such that $C \propto \sigma_{\mathrm{sc}} N_{\mathrm{trips}}/A_{\mathrm{eff}} \propto Q\lambda_{eg}^3/V_{\mathrm{eff}}$. Here $Q = \omega_c/\kappa$ is the quality factor of the cavity (we assume the cavity resonance frequency ω_c is comparable to ω_{eg}), and V_{eff} is the cavity mode volume. Thus the desired ingredients for efficient interaction are a long photon lifetime and high degree of spatial confinement of light.

As cavity QED constitutes such an important paradigm within atomic physics, we will present some key theoretical aspects here, followed by a discussion of experimental state of the art. This will enable a more detailed comparison with nanophotonics setups later. For additional details on cavity QED, we refer to Haroche and Raimond (2006) and Reiserer and Rempe (2015). The Jaynes-Cummings model (Jaynes and Cummings, 1963) is a model Hamiltonian that describes the interaction of a single atom and photons occupying a single optical mode and is given by

$$H_{\mathrm{JC}} = \hbar\delta_{\mathrm{JC}}\sigma_{ee} + \hbar g_{\mathrm{JC}} \cos kx(\sigma_{eg}a + a^\dagger\sigma_{ge}). \tag{1}$$

Here the atomic operators are defined as $\sigma_{\alpha\beta} = |\alpha\rangle\langle\beta|$ and $\delta_{\mathrm{JC}} = \omega_{eg} - \omega_c$ is the frequency difference between the cavity resonance and atomic transition. The cavity mode is taken to be a standing wave, although in this section we assume that the atomic position x satisfies $\cos kx = 1$, i.e., the atom sits at an antinode. On resonance ($\delta_{\mathrm{JC}} = 0$), the Hamiltonian allows for an atom to transition from its ground state to excited state by absorbing a cavity photon and to subsequently reemit it at a rate g_{JC} (the so-called vacuum Rabi splitting). In terms of microscopic parameters, g_{JC} is related to the atomic dipole matrix element $\wp = \langle e|\mathbf{d}|g\rangle$ and mode volume by $g_{\mathrm{JC}} = \wp\sqrt{\omega/2\epsilon_0\hbar V_{\mathrm{eff}}}$. In general, H_{JC} conserves the total number of excitations (atomic excitations plus photons) and is thus easily diagonalizable.

One relevant limit is when the cavity detuning $|\delta_{\mathrm{JC}}|$ is large compared to g_{JC}, in which case the atom and photons nearly decouple. Then, for one total excitation, one of the eigenstates is mostly an atomic excitation $|\psi_+\rangle \approx |e,0\rangle - (g_{\mathrm{JC}}/\delta_{\mathrm{JC}})|g,1\rangle$ with corresponding eigenvalue $\omega_+ \approx \delta_{\mathrm{JC}} + g_{\mathrm{JC}}^2/\delta_{\mathrm{JC}}$. Here $|n\rangle$ denotes the Fock state of n cavity photons. The excited-state frequency is shifted by an amount $g_{\mathrm{JC}}^2/\delta_{\mathrm{JC}}$ compared to its bare value, due to the dressing by a small amount $(g_{\mathrm{JC}}/\delta_{\mathrm{JC}})^2$ of photon population. For multiple atoms coupled to the cavity at positions x_i, this common virtual photon gives rise to an effective "spin" interaction between atoms if the photon is integrated out (Goldstein and Meystre, 1997),

$$H_{\mathrm{JC,eff}} = \sum_{jl} \frac{g_{\mathrm{JC}}^2}{\delta_{\mathrm{JC}}} \cos kx_j \cos kx_l \sigma_{eg}^j \sigma_{ge}^l. \tag{2}$$

This Hamiltonian describes the exchange of atomic excitations and is infinite range, as the photon mediating the interaction resides equally between the two cavity mirrors and thus the physical separation between the atoms is irrelevant (aside from the standing-wave modulation).

Besides the ideal coherent evolution under $H_{\mathrm{JC,eff}}$, a realistic system also exhibits two fundamental dissipation mechanisms [Fig. 2(b)]. First, an excited atom can spontaneously emit a photon into free space at a rate Γ', since the cavity is not closed. For realistic Fabry-Perot cavities in the optical domain, the cavity mode subtends a small fraction of the total solid angle into which the atom can emit and thus Γ' is comparable to the vacuum emission rate $\Gamma_0 = \omega_{eg}^3\wp^2/(3\pi\epsilon_0\hbar c^3)$. In addition, the cavity photon can decay at a rate κ. We now provide an example of how the cooperativity emerges as the figure of merit when optimizing a desired process in the presence of losses. In particular, we consider two atoms coupled via $H_{\mathrm{JC,eff}}$ and investigate the maximum spin-exchange fidelity to the state $|ge\rangle$, assuming that the initial state is $|eg\rangle$. The time for exchange is given by $\tau \approx \pi\delta_{\mathrm{JC}}/2g_{\mathrm{JC}}^2$, while the loss rate is $\Gamma_{\mathrm{tot}} \approx \Gamma' + \kappa(g_{\mathrm{JC}}/\delta_{\mathrm{JC}})^2$ (the weighted average of the atomic and photonic population and their respective decay rates). The total error probability $\mathcal{E} \approx \tau\Gamma_{\mathrm{tot}}$ during the exchange can be minimized with respect to δ_{JC} to yield $\mathcal{E}_{\mathrm{min}} = \pi/\sqrt{C}$, where $C \equiv g_{\mathrm{JC}}^2/\kappa\Gamma'$ is the single-atom cooperativity. Since $\Gamma' \approx \Gamma_0$, one can readily show that $C \propto \lambda_{eg}^3 Q/V_{\mathrm{eff}}$, which confirms the validity of the intuitive scattering cross-section argument presented earlier.

In conventional Fabry-Perot cavities (Miller *et al.*, 2005; Reiserer and Rempe, 2015), it is possible to achieve a cooperativity on the order of $C \sim 10$–100. As cavities in these experiments already support an extremely high finesse of $N_{\mathrm{trips}} > 10^5$, in the past 20 years numerous groups have begun exploring different types of cavities in order to reduce the mode volume V_{eff}. These included whispering-gallery-mode resonators (Vernooy *et al.*, 1998; Aoki *et al.*, 2006; O'Shea *et al.*, 2013; Shomroni *et al.*, 2014) and fiber-based cavities (Colombe *et al.*, 2007; Volz *et al.*, 2011; Kato and Aoki, 2015), which increased cooperativities by an order of magnitude. These miniaturized cavities were also an important stepping stone toward nanophotonic systems.

(iii) Atomic ensembles: A third approach to increasing the interaction probability of a photon with atomic media is to use a large number of atoms N_a, in which case the resulting figure

of merit is $\mathrm{OD} = (\sigma_{\mathrm{sc}}/A_{\mathrm{eff}})N_a$. This defines the "optical depth" of an atomic ensemble and characterizes the degree of exponential attenuation in transmitted intensity for a resonant incident beam $T = \exp(-\mathrm{OD})$. While exponential attenuation (arising from scattering into other directions) is not particularly useful, it can be shown that the optical depth still retains importance once the ensemble is functionalized (Hammerer, Sørensen, and Polzik, 2010) (for example, by using three-level atoms and implementing electromagnetically induced transparency, discussed later). Even when functionalized, however, an ensemble with high optical depth generally does not have the same power as a high-cooperativity cavity. In particular, a single two-level atom is intrinsically nonlinear and generates nonclassical states of light, and increasing the cooperativity in cavity QED enables one to directly exploit this property. However, increasing OD with many atoms typically makes the system highly linear (as now up to $\sim N_a$ photons are needed to saturate all the atoms). Thus, weak light pulses interacting with atomic ensembles are usually characterized by linear or Gaussian dynamics (Hammerer, Sørensen, and Polzik, 2010). This regime in itself has many applications, including quantum memories for light (Fleischhauer and Lukin, 2000; Liu *et al.*, 2001; Julsgaard *et al.*, 2004; Choi *et al.*, 2008), spin squeezing (Kuzmich, Mandel, and Bigelow, 2000), or probabilistic schemes for quantum information processing (Duan *et al.*, 2001; Kuzmich *et al.*, 2003; Chaneliere *et al.*, 2005; Duan and Monroe, 2008). However, demonstrated nonlinear interaction strengths thus far in atomic ensembles (aside from Rydberg gases, described next) are about 2 orders of magnitude below that needed for single photons to interact (Bajcsy *et al.*, 2009). It should be noted that although a single atom can have a reasonably large optical depth of $\mathrm{OD} \sim 0.1$ (Darquie *et al.*, 2005; Tey *et al.*, 2008), this per-atom OD cannot be extended to ensembles as a tightly focused beam rapidly diverges in area (Tanji-Suzuki *et al.*, 2011; Baragiola *et al.*, 2014; Qi *et al.*, 2016). The challenge of achieving high atomic densities and long interaction lengths typically limits free-space ensembles to optical depths of $\mathrm{OD} \lesssim 10^2$.

(iv) Rydberg gases: As argued, an atomic ensemble typically enables efficient interactions with single photons at the cost of making the system highly linear. A remarkable approach to achieving strong nonlinear interactions in ensembles was pursued in recent years (Lukin *et al.*, 2001). The key idea is to utilize the efficient atom-light interactions to map single photons into highly excited Rydberg levels of atoms (Saffman, Walker, and Mølmer, 2010), as illustrated in Fig. 2(d) (Pritchard, Weatherill, and Adams, 2013; Firstenberg, Adams, and Hofferberth, 2016; Murray and Pohl, 2016). Here photons in a probe beam near resonance with the $|g\rangle - |e\rangle$ transition can be coherently absorbed into a Rydberg state $|r\rangle$, through a two-photon transition mediated by a strong classical pump beam Ω. The transfer of an atom into the metastable state $|r\rangle$ suppresses the usual strong absorption and rescattering associated with two-level atoms and results in the process of "electromagnetically induced transparency" (EIT) (Fleischhauer, Imamoglu, and Marangos, 2005). This process is efficient only if the sum of probe and pump frequencies matches the transition energy from $|g\rangle$ to $|r\rangle$. Once a Rydberg excitation is created, however, it shifts the energy of the Rydberg level of nearby atoms by an amount $V(r)$ due to strong van der Waals interactions. This shift prevents the resonance condition from being matched for a second probe photon, within a certain Rydberg "blockade" radius r_b. This second photon effectively sees only a two-level medium of $|g\rangle$-$|e\rangle$ and is strongly scattered. The resulting output state of the probe beam can then exhibit nonclassical correlations, as it contains only single photons within a given spatial region (Pritchard *et al.*, 2010; Dudin and Kuzmich, 2012; Peyronel *et al.*, 2012). This Rydberg blockade was successfully used to realize effects such as single-photon switching (Gorniaczyk *et al.*, 2014; Tiarks *et al.*, 2014).

III. A NEW WAY FORWARD: ATOMS AND NANOPHOTONICS

In the previous section, we presented an overview of the (mostly orthogonal) approaches toward achieving efficient atom-photon interactions: tight focusing of beams, multiple round-trips, many atoms, and atom-atom interactions, and we discussed some of the technical challenges faced in these various strategies. This background facilitates a comparison with nanophotonic systems. In this section, we begin by introducing some important nanophotonic structures, such as nanofibers, photonic crystal waveguides, and photonic crystal cavities. At a minimum, directly mapping existing paradigms (such as cavity QED) onto such structures can result in significantly improved figures of merit, due to factors such as strong confinement of optical fields. We will discuss the current and potential figures of merit associated with nanophotonic structures here. Importantly, however, we will also see that nanophotonic systems provide the opportunity to engineer the dispersion and modal properties of light and the dimensionality in which atoms and photons "see" each other. These considerations will be important in later sections, when we discuss how one can create new paradigms for atom-light interactions, which have no prior analog in atomic physics and quantum optics.

A. Overview of nanophotonics

Perhaps the simplest nanophotonic structure, which serves as a starting point to understand more complex structures, is an optical nanofiber [Fig. 3(a)]. In a ray optics picture, a fiber guides light within a high refractive index core, surrounded by a lower index cladding (in our case vacuum), through total internal reflection. The dispersion relation of the guided mode frequency f versus wave vector k along the propagation axis of a cylindrical nanofiber of radius $r_{\mathrm{fiber}} = 250$ nm is illustrated in Fig. 3(b). For sufficiently small core radii $kr_{\mathrm{fiber}} \lesssim 2$, the fiber supports only a single transverse spatial mode, labeled "HE11" in the figure, at a given frequency. Interestingly, there is no cutoff for small radius (in contrast to a microwave waveguide) (Jackson, 1999). To respect the diffraction limit of $A_{\mathrm{eff}} \gtrsim \lambda^2$, a significant evanescent field then forms *outside* the core, which can extend in the transverse direction far beyond the radial size r_{fiber} (Le Kien, Balykin, and Hakuta, 2004), as shown in Fig. 3(c). As we discuss later, this evanescent field provides a mechanism to trap atoms in

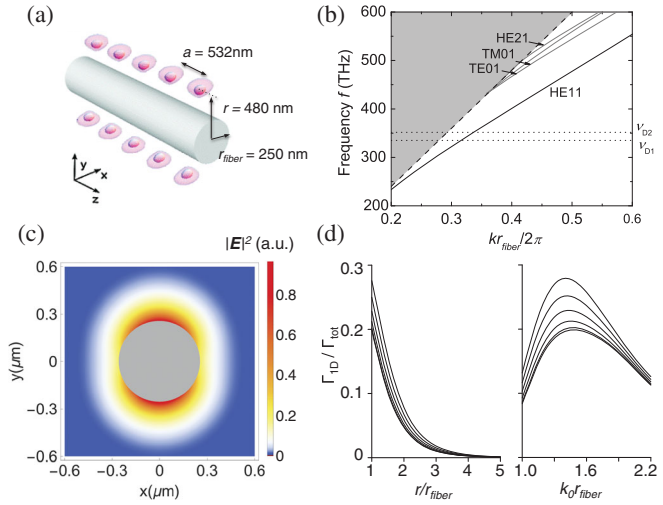

FIG. 3. (a) Schematic of a SiO_2 nanofiber of radius $r_{\text{fiber}} = 250$ nm, with atoms trapped approximately 230 nm from the surface. Adapted from Vetsch *et al.*, 2010. (b) Dispersion relation of the guided mode frequency f vs axial wave vector k (in units of $2\pi/r_{\text{fiber}}$) for the nanofiber. For sufficiently small fibers or low frequencies, all modes except the HE11 mode are cut off. The transition frequencies associated with the Cs D1 and D2 lines are also shown for reference. (c) Intensity distribution $|E|^2$ (in arbitrary units) for the fundamental HE11 mode of the nanofiber (Le Kien, Balykin, and Hakuta, 2004). (d) (Left) Ratio of emission rate Γ_{1D} into the guided mode to total emission Γ_{tot} of an atom trapped near a nanofiber of radius $r_{\text{fiber}} = 200$ nm, as a function of dimensionless distance r/r_{fiber}. The curves correspond to different magnetic sublevels of Cs. (Right) Same ratio, calculated as a function of fiber radius (normalized by the resonant wave vector $k_0 = \omega_{eg}/c$ in vacuum), for an atom on top of the fiber surface. From Le Kien *et al.*, 2005.

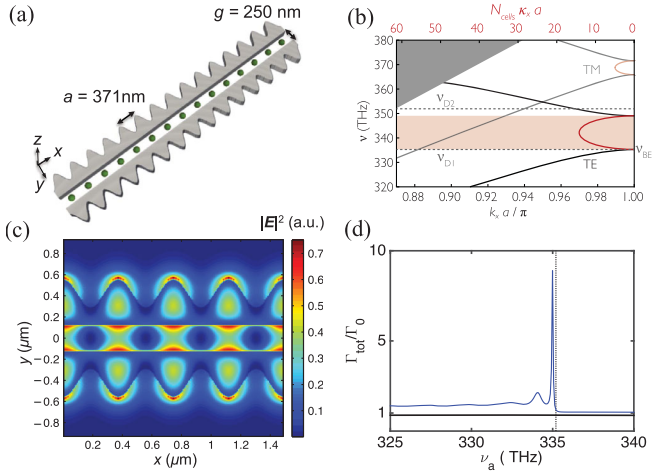

FIG. 4. The quasi-1D "alligator" photonic crystal waveguide (APCW). (a) Schematic illustration of a section of the APCW (Si_3N_4 dielectric) and its dimensions, with one atom trapped per unit cell (green spheres). (b) Dispersion relation of frequency ν vs wave vector k_x (normalized by π/a, where a is the lattice constant) for the lowest order TE and TM modes (black and gray curves, respectively). A band gap (red shaded region) appears for the TE mode near the D1 and D2 transition frequencies of atomic Cs (dotted lines), in which the TE field cannot propagate but evanescently decays. The decay constant κ_x (normalized by a^{-1}) is shown in red. From Hood *et al.*, 2016. (c) Intensity profile $|E|^2$ (in arbitrary units) for the TE mode at the lower band edge. (d) Total spontaneous emission rate Γ_{tot} (into both free space and guided modes), normalized by the vacuum rate Γ_0, for a single atom located at the center of a unit cell in the middle of a APCW composed of $N_{\text{cells}} = 150$ unit cells. The dashed vertical line indicates the frequency of the band edge.

the vacuum region near the fiber and create high interaction probability between individual atoms and resonant propagating photons guided within the fiber.

The dispersion relation of a fiber is featureless over very large bandwidths, indicating its ability to guide light of very different wavelengths and with little distortion. On the other hand, for many applications within classical optics it might be desirable to tailor the dispersion relation, for example, to realize frequency filters or compact delay lines. One powerful way to modify the dispersion relation of a translationally invariant fiber or dielectric waveguide is to periodically modulate the dielectric profile $\epsilon(r)$ along the propagation axis [such as by sinusoidal variation of the structure width as illustrated in Fig. 4(a)], thus realizing a "photonic crystal" waveguide (PCW) (Joannopoulos *et al.*, 2008). While a single cycle of modulation behaves as a simple scatterer for guided fields, the multiple interference in scattering from a periodic array can behave in a much more complex manner. In this case, Bloch's theorem serves as a convenient way to describe propagation through this periodic "potential." In particular, the dispersion relation $\omega(k)$ of guided modes is characterized by a Bloch wave vector k along the propagation axis (taking the values $|k| \leq \pi/a$ in the first Brillouin zone) and set of bands [see Fig. 4(b)]. In analogy with electrons propagating through a periodic crystal potential in solid-state systems, a characteristic feature of band structure is the emergence of band gaps, a frequency range over which no guided modes exist, due to the strong constructive interference in reflection from the periodic dielectric modulation. An interesting feature of a guided band, as it approaches in frequency toward a band edge, is that its group velocity $v_g = d\omega/dk$ can in principle approach zero. This reduced propagation speed arises due to multiple reflections that light makes, while it maintains a net propagation direction.

Another structure of interest is a photonic crystal cavity (PCC); see Fig. 5. Such a structure can be realized by introducing a local defect into a PCW, for example, by locally altering the size of the periodic modulation of the waveguide as seen in Fig. 5(b). This defect can seed a set of discrete cavity modes whose resonance frequencies are situated within the band gap of the surrounding structure, thus spatially localizing the modes around the defect. The associated mode volumes can easily reach the diffraction limit $V_{\text{eff}} \lesssim \lambda^3$. Thus, such a platform has proven to be attractive in recent years for achieving strong light-matter interactions in a number of settings beyond atoms. For example, the structure in Fig. 5(b) enables strong optomechanical coupling between photons and a colocalized mechanical mode of the structure (Safavi-Naeini *et al.*, 2011).

Finally, it should be mentioned that the concepts associated with the progression from nanofibers to photonic crystal

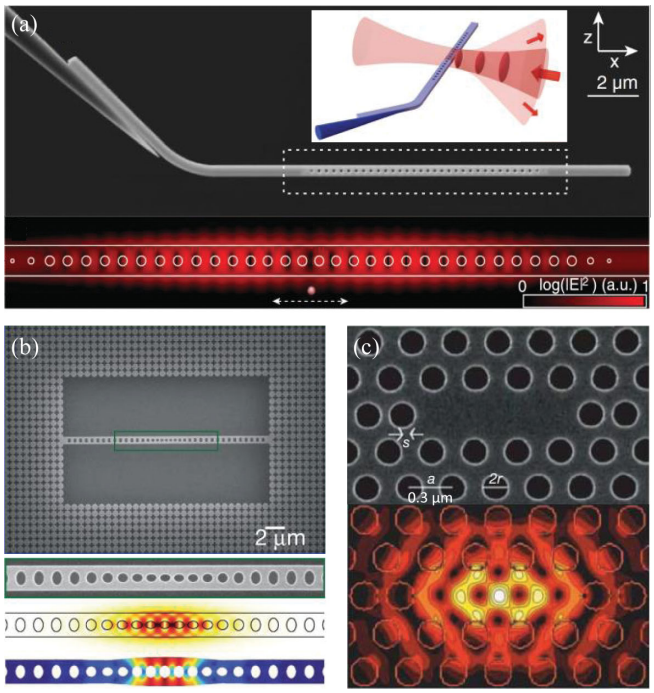

FIG. 5. Photonic crystal cavities. (a) A scanning electron microscope (SEM) image (upper panel) and simulation of mode intensity (lower) of a defect cavity defined in a one-dimensional photonic crystal beam. On the left of the upper panel is a tapered nanofiber used for coupling light into and out of the cavity. In Thompson *et al.* (2013), atoms were optically trapped nearby in the interference fringe formed by reflecting a tightly focused beam from the structure (inset). (b) An "optomechanical crystal" SEM image of a defect cavity in a one-dimensional photonic crystal beam. The panel below shows a zoom-in of the defect region, with variations in the sizes of the holes. This defect creates localized resonances both for photons and phonons as seen in the two bottom panels illustrating the cavity mode intensity and acoustic "breathing" modes. From Safavi-Naeini *et al.*, 2011. (c) Cavity mode defined in a 2D photonic crystal membrane. In Yoshie *et al.* (2004), the defect is formed by the omission of three holes from the otherwise periodic structure.

waveguides to cavities also extend to two-dimensional structures. In particular, a thin film dielectric membrane supports a set of modes guided by total internal reflection, and adding a dielectric modulation such as a set of holes results in a photonic crystal structure described by a two-dimensional Bloch band structure (Painter *et al.*, 1999; Joannopoulos *et al.*, 2008). Likewise, adding a defect to such a structure, such as by omitting a set of holes over a finite region [see Fig. 5(c)], results in a discrete cavity mode confined to this region (Yoshie *et al.*, 2004), whose mode volume can also be diffraction limited. We now discuss the interface of atoms with these various types of nanophotonic systems.

B. Optical nanofibers

While a substantial single-atom interaction probability of $P \sim 0.1$ is achievable using a tightly focused laser beam and one trapped atom (Darquie *et al.*, 2005; Tey *et al.*, 2008; Hetet *et al.*, 2011), this technique does not extend to many atoms due to the rapid divergence of the beam waist under tight focusing. Researchers (Nayak *et al.*, 2007) thus began to explore techniques to maintain the tight confinement of beams over long distances through the use of optical nanofibers and thereby potentially realize significant optical depths in atomic ensembles using relatively few atoms.

As illustrated in Fig. 3(c), for a SiO_2 nanofiber of radius $r_{\text{fiber}} = 200$ nm, a significant amount of the guided mode intensity extends evanescently into the surrounding vacuum region. Because of the diffraction-limited mode area $A_{\text{eff}} \sim \lambda_{eg}^2$, an atom within this evanescent tail can have a large interaction probability with a single guided photon on resonance. Atom-light interactions in nanofibers were first observed using untrapped atoms in an atomic gas surrounding the nanofiber (Nayak *et al.*, 2007). A major breakthrough occurred when it was demonstrated that $N_a \sim 10^3$ atoms could be cooled into lattice sites created by a two-color trap from a surrounding magneto-optical trap (MOT) (Vetsch *et al.*, 2010), which dramatically increased the number of atoms interacting with the guided mode, as illustrated schematically in Fig. 3(a) (see Sec. VI for more details on trapping). Initial experiments observed optical depths per atom of OD = 0.0064 (Vetsch *et al.*, 2010) and OD = 0.08 (Goban *et al.*, 2012). With $N_a \approx \{4000, 800\}$ atoms, respectively, trapped along the nanofiber in these experiments, the overall optical depths were OD $\approx \{13, 66\}$, which compares favorably to typical cold-atom ensembles in free space. The per-atom optical depth in these experiments arises from the efficient emission rate Γ_{1D} into the guided modes compared to free space (Γ') as OD $\approx 2\Gamma_{1D}/\Gamma'$ for $\Gamma_{1D} \ll \Gamma'$ (Asenjo-Garcia, Hood *et al.*, 2017). The theoretically calculated ratio of guided to total emission (Le Kien *et al.*, 2005) $\Gamma_{1D}/\Gamma_{\text{tot}}$ is plotted in Fig. 3(d). The ratio is evaluated both as a function of distance to the fiber (left panel), which clearly shows the evanescent decay of the field away from the fiber surface, and as a function of fiber radius (right panel), which exhibits a maximum when the field confinement A_{eff} is optimized. Beyond these proof-of-principle interfaces of atoms and nanofibers, some experiments have proceeded recently to implement basic quantum coherent phenomena, such as slow light and coherent photon storage (Gouraud *et al.*, 2015; Sayrin, Clausen *et al.*, 2015; Solano *et al.*, 2017).

C. 1D and 2D photonic crystal waveguides

The ability to tailor the modal properties and dispersion relation of a PCW significantly beyond that of a conventional waveguide also offers a greatly expanded toolbox for controlling atom-light interactions. Recall that single photons in a nanofiber interface are limited to a single-atom optical depth of OD ~ 0.1 on a single pass. This coupling can be greatly enhanced by exploiting the reduced group velocity $v_g = d\omega/dk$ of PCW guided modes near a band edge (John and Quang, 1994; Lund-Hansen *et al.*, 2008). As discussed earlier, this slow group velocity arises as light reflects multiple times off the dielectric modulation while it propagates. Thus, a photon effectively experiences an extended interaction time with an atom relative to free space, which is given by the group index $n_g = c/v_g$ for the PCW. The emission rate into

the waveguide is subsequently enhanced by an approximate factor $\Gamma_{1D} \to n_g\Gamma_{1D}$ (with a corresponding enhancement $\mathrm{OD} \to n_g\mathrm{OD}$ while $\Gamma_{1D} \lesssim \Gamma'$). Such an enhancement, first seen experimentally with quantum dot emitters (Lund-Hansen *et al.*, 2008; Arcari *et al.*, 2014), becomes particularly interesting in the limit that $\Gamma_{1D} \gg \Gamma'$, such that free-space coupling is negligible. This essentially realizes quantum electrodynamics in propagating 1D channels, for which rich theoretical phenomena have been predicted (Shen and Fan, 2005; Chang *et al.*, 2007; Ramos *et al.*, 2014; Ringel, Pletyukhov, and Gritsev, 2014) but thus far largely lacks experimental realization.

In the context of atoms, the first experiments to observe enhanced emission associated with a band edge used a so-called "alligator" photonic crystal waveguide (APCW), illustrated in Fig. 4(a). The APCW consists of two parallel, modulated silicon nitride (Si_3N_4) dielectric waveguides, which are in close enough vicinity that their modes interact and hybridize. The APCW is designed such that the edge of a transverse-electric- (TE-) like band aligns closely with the atomic transition frequency of Cs. The guided mode intensity profile at the band edge, shown in Fig. 4(c), exhibits a high concentration between the two waveguides and further increases the interaction probability in the case that a single atom can be localized there.

Single atoms have been trapped along such an APCW structure and enhanced values with $\Gamma_{1D}/\Gamma' \approx 1$ have been achieved (Goban *et al.*, 2015). For average atom number $\bar{N}_A \approx 3$, superradiant emission has been observed with rates in good agreement with predictions obtained from numerical simulations. Some representative results from these simulations, discussed further in Sec. V, are shown in Fig. 4(d). Here the predicted single-atom ratio of $\Gamma_{\mathrm{tot}}/\Gamma_0 = (\Gamma_{1D} + \Gamma')/\Gamma_0$ is plotted, as a function of detuning from the band edge, for the actual finite system. The general trend of enhancement for Γ_{1D} near the band edge is observed; however, the ideal (unlimited) enhancement by $n_g = c/v_g$ due to $v_g \to 0$ at the band edge of an infinite structure is interrupted by a set of resonances associated with the finite length and imperfect impedance matching at the ends. Improved trapping and design of PCWs could lead to values $\Gamma_{1D}/\Gamma' \sim 10^2$ (Zang *et al.*, 2016).

While much of quantum optics with atoms has focused on enhancing the interactions with preferred optical modes, PCWs offer the opportunity to simultaneously engineer structures with suppressed emission Γ' into undesired guided modes and free space. While such suppression has been observed in atomic physics (Haroche and Kleppner, 1989), the effect is negligible in conventional optical cavities (e.g., spherical mirror Fabry-Perot resonators) due to the small solid angle subtended by the cavity mode (i.e., Γ' deviates from the rate Γ_0 of an isolated atom by only a part in 10^5) (Miller *et al.*, 2005). However, due to their nanoscopic unit cells, PCWs capture a large solid angle of atomic radiative emission. Furthermore, the dielectric medium surrounding trapped atoms can be engineered to have a band gap at frequencies around relevant atomic transitions, thereby suppressing what would otherwise be free-space loss. Analogous effects have already been exploited in quantum dots coupled to PCWs (Arcari *et al.*, 2014); here it is estimated that the structure suppresses Γ' by an order of magnitude and leads to record ratios of Γ_{1D}/Γ' in the optical domain.

Extension to 2D PCWs can lead to strong atom-field interactions and rich physics resulting from band structure engineering. For example, the aforementioned near-unity quantum dot-PCW coupling efficiency was in fact realized in a 1D line defect embedded in a 2D photonic crystal [shown similarly in Fig. 3(c) but with an entire line of missing air holes]. Because of strong mode mixing in line defects (Notomi *et al.*, 2001; Li *et al.*, 2008), it has been experimentally demonstrated that a very flat band resulting from an avoided band crossing can exhibit extremely slow light propagation ($v_g \approx c/300$) (Vlasov *et al.*, 2005) with a broad bandwidth. This effect could in principle be utilized to further improve upon the atom-photon interaction probability P. Separately, it has been proposed and experimentally demonstrated that a complete band gap for both TE and transverse-magnetic (TM) polarizations can be engineered in a 2D PCW (Cassagne, Jouanin, and Bertho, 1996; Wang *et al.*, 2001; Takayama *et al.*, 2005). Embedding an atomic transition in a full photonic band gap could provide better suppression of the unwanted emission rate Γ' and enables the exploration of coherent atom-photon interactions inside a band gap as discussed in the following sections.

D. Nanophotonic optical cavities

As described in Sec. II, for more than a decade numerous groups have been exploring alternatives to Fabry-Perot cavities for efficient atom-light interactions, which would offer reduction in mode volumes V_{eff} and a corresponding increase in vacuum Rabi splittings g_{JC} and cooperativities C (Vernooy *et al.*, 1998; Aoki *et al.*, 2006; Volz *et al.*, 2011; O'Shea *et al.*, 2013; Shomroni *et al.*, 2014). Parallel efforts also took place to integrate atomlike solid-state emitters such as quantum dots with small lithographically fabricated cavities (Pelton *et al.*, 2002), and PCCs with diffraction-limited mode volumes rapidly emerged as a leading approach (Yoshie *et al.*, 2004; Badolato *et al.*, 2005; Fushman *et al.*, 2008; Laucht *et al.*, 2009). Quantum dot-coupled cavities in GaAs now routinely reach $Q > 10^4$ (Laucht *et al.*, 2009), while advances in design (Srinivasan and Painter, 2002; Akahane *et al.*, 2005) and fabrication (Asano, Song, and Noda, 2006; Sekoguchi *et al.*, 2014) have now led to observations of $Q \approx 10^7$ in bare silicon PCCs (Sekoguchi *et al.*, 2014).

Projection of these parameters to atomic systems would lead to unprecedented figures of merit compared to Fabry-Perot cavities (see Fig. 6). For example, for an atomic cesium transition, a well-designed cavity with diffraction-limited mode volume $V_{\mathrm{eff}} < \lambda_{eg}^3$ would yield a vacuum Rabi splitting of $g_{\mathrm{JC}}/2\pi \sim 10$ GHz (Hung *et al.*, 2013; Douglas *et al.*, 2015), leading to a cooperativity of $C \sim 10^4$ for a cavity of $Q = 2 \times 10^5$. The first experiments to interface single atoms with PCCs defined in Si_3N_4 beams were reported by Thompson *et al.* (2013) and Tiecke *et al.* (2014). Here single atoms were trapped in tightly focused optical tweezers, and the beam was subsequently steered over the PCC. Interference between the beam and its reflection yields a periodic intensity modulation above the structure, and the atom can be controllably loaded into the first fringe about 200 nm above the

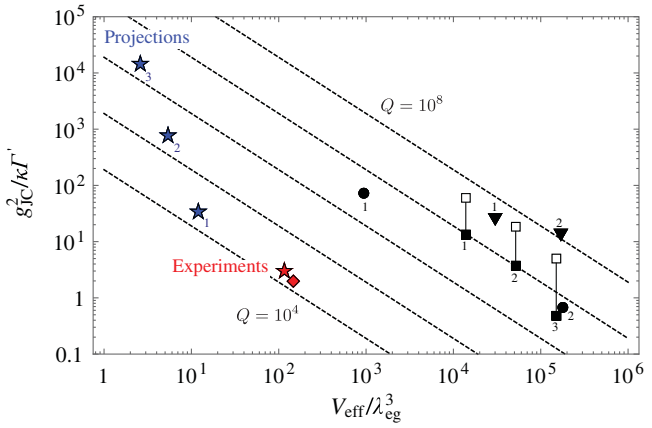

FIG. 6. Comparison of cooperativity factors $C = g_{1C}^2/\kappa\Gamma'$ for different cavity QED and atomic interfaces. With initial designs and reasonable $Q \approx 20\,000$, a nanoscopic photonic crystal cavity (red diamond) (Tiecke *et al.*, 2014) and an APCW band-gap atom cavity (red star) (Hood *et al.*, 2016) have already achieved cooperativity parameters $C > 1$ that are comparable with state-of-the-art macroscopic and microscopic resonators, which include mirror Fabry-Perot cavities [triangles, 1 (Miller *et al.*, 2005); 2 (Sames *et al.*, 2014)], fiber-based cavities [circles, 1 (Colombe *et al.*, 2007); 2 (Kato and Aoki, 2015)], microtoroid, microsphere, and bottle whispering-gallery-mode resonators [squares, 1 (Aoki *et al.*, 2006); 2 (Shomroni *et al.*, 2014); 3 (O'Shea *et al.*, 2013); open squares: projections using intrinsic Q]. Here the dashed lines mark constant quality factors $Q = 10^4$, 10^5, 10^6, 10^7, and 10^8 in increasing order. Blue stars mark projected improvements by (1) improved trap loading to minimize the effective mode area (Hung *et al.*, 2013; Goban *et al.*, 2015); (2) increased quality factor to $Q = 2 \times 10^5$ as well as 10-fold reduction in the band curvature to reduce effective mode volume (Douglas *et al.*, 2015; Zang *et al.*, 2016); (3) further suppression of Γ' (Hung *et al.*, 2013; Gonzalez-Tudela, Hung *et al.*, 2015).

device [Fig. 5(a), also see more detailed discussion of trapping in Sec. VI]. These initial structures demonstrated values of $g_{1C}/2\pi \sim 1$ GHz (lower than the maximum as the atom is trapped in the evanescent tail of the cavity field) and cavity dissipation-limited quality factors of $Q \sim 10^5$. The potential of PCCs for cavity QED is seen in the demonstration of a quantum phase switch (Tiecke *et al.*, 2014) just one year after initial proof-of-principle coupling.

E. Imperfections

Thus far, our discussion on atom-photon interactions in nanophotonics largely assumes "perfect" structures. However, nanofibers, 1D and 2D PCWs, PC cavities, and other structures push state-of-the-art capabilities on various fronts of fabrication and characterization. The consequences of imperfections can indeed influence the resulting atom-photon interactions. Perhaps the most prominent and universal effect that can arise is Anderson localization, wherein scattering disorder can cause light that would be guided in a perfectly periodic structure to become confined over some characteristic "localization length" L_A. Anderson localization in PCWs has already been extensively studied (Topolancik, Ilic, and Vollmer, 2007; Mazoyer, Hugonin, and Lalanne, 2009; Patterson *et al.*, 2009; Garcia *et al.*, 2010); we will not repeat the rather technical details here. To minimize such effects, it is certainly important that L_A exceeds the system size or any emergent length scale over which atoms interact via photons. On the other hand, Anderson localization may also prove to be a feature of such systems allowing the investigation of atom-photon interactions in disordered environments. A more elaborate discussion of Anderson localization relevant to atomic physics can be found by Goban *et al.* (2014) and Douglas *et al.* (2015).

A second source of imperfection arises from defects due to atomic adsorption on the surface of the nanophotonic structure. There are two possible impacts. First, it is known that surface-adsorbed alkali atoms act as electric dipoles that generate electric field fluctuations, potentially contributing to decoherence and heating of trapped atoms near the surface (McGuirk *et al.*, 2004). However, for insulating dielectric materials such as silica and silicon nitride that do not strip out the valence electron from an adsorbed atom, only a small electric dipole moment will be induced. Experimental results by McGuirk *et al.* (2004) suggest that a single adsorbed atom generates an electric field $< 0.2\ \mu$V/cm at a distance of around 10 μm from a glass surface. Assuming a point dipole source, this translates to an estimated electric field strength of $\sim$0.2 V/cm at a distance of 100 nm from the surface, leading to an insignificant static dipole-dipole energy shift $< h \times 2$ mHz (due to one surface adatom) on trapped atoms.

The second and perhaps the most prominent impact due to surface adsorption is the modification of dielectric properties, such as the effective refractive index. As the number of adsorbed atoms increases, the photonic band edge or a high-Q optical resonance can be shifted significantly (Barclay *et al.*, 2006). Surface adsorption can also induce optical loss and deteriorate the mode quality (Ritter *et al.*, 2015). A workaround is by constantly heating the nanostructure to remove surface-adsorbed atoms. A more effective and permanent solution could be to coat the nanostructure with an atomically thin protective layer such as sapphire (Al_2O_3), which has been reported to significantly increase the lifetime of a nanostructure against surface adsorption (Ritter *et al.*, 2016).

Beyond nanophotonic imperfections, nonideal atomic localization can also result in imperfect atom-photon interactions. This is due to rapid variation in an electric field mode profile near a nanostructure [Figs. 3(c) and 4(c)]. Specifically, in-trap atomic thermal motion can cause Γ_{1D} (or g_{1C}) to vary significantly [e.g., by a factor $\sim O(2)$ in experiments with temperature $\sim$100 μK due to motion in the axial and transverse directions relative to the nanostructure]. Moreover, atomic thermal motion also limits the coherence time. In a nanofiber, Reitz *et al.* (2013) reported that trap inhomogeneous broadening and trap heating can reduce the coherence time $T_2 < 1$ ms. In order to remedy these imperfections, further cooling in these tight traps may be necessary. Recently, it was demonstrated that the unique polarization characteristics of tightly confined fields around an optical nanofiber allow for the implementation of novel cooling mechanisms that bring the motion of trapped atoms close to their quantum ground states (Albrecht *et al.*, 2016).

Moreover, several new paradigms require arrays of trapped atoms at specific lattice constants. As discussed in Sec. VII, the

ideal lattice spacing can be realized either by PCW band structure engineering (Hung *et al.*, 2013) or by using near-detuned traps (Corzo *et al.*, 2016) or structuring pulses (Sorensen *et al.*, 2016) as demonstrated in recent nanofiber experiments. A much more stringent requirement, however, must be considered in Sec. IX, where, for example, unit filling of lattice sites is required to explore spin models. This imposes greater experimental challenges since laser cooling fills individual sites randomly with either 0 or 1 atoms due to a collisional blockade (Schlosser *et al.*, 2001). A small number of uniformly filled sites may be attainable using an auxiliary laser beam to modify in-trap collision dynamics (Grünzweig *et al.*, 2010; Lester *et al.*, 2015). To form a large atomic lattice, a moving "sorter" beam (Barredo *et al.*, 2016) or a reconfigurable tweezer array (Endres *et al.*, 2016) may be implemented as both schemes have successfully achieved large defect-free lattices in free space.

IV. A SURPRISING FUTURE FOR ATOM-PHOTON PHYSICS

Having described how nanophotonic systems can push the figures of merit associated with conventional paradigms for atom-light interactions, we now devote the remainder of this Colloquium to how such systems can realize new paradigms. These paradigms potentially provide novel routes toward applications such as manipulation of quantum information, or toward creating exotic many-body states of light and matter. In this section, we give a brief summary for more casual readers of these possibilities and intuitive descriptions of the key underlying physics. Subsequent sections provide a more rigorous discussion.

A major historical motivation for the migration to nanofibers and photonic crystal waveguides is to generate a favorable collection efficiency of emission from a single atom into the preferred guided modes over unwanted free-space emission. In recent years, it has been recognized that with more atoms, one can take advantage of this large, *collective* dissipation channel to generate and manipulate quantum coherence among atoms and interesting quantum optical states. An additional tuning knob, which arises naturally in nanophotonic systems, is the ability to utilize the polarization of tightly confined fields to realize chiral dissipation channels, in which an atom emits preferentially in one direction even if the nanophotonic device itself is mirror symmetric. The classes of novel phenomena and applications that have emerged based upon collective dissipation and "chiral" quantum optics are introduced in Secs. IV.A and IV.B, respectively. Perhaps counterintuitively, novel paradigms can also arise by *turning off* emission into a nanophotonic structure. In particular, by aligning a transition within the band gap of a photonic crystal, an excited atom cannot emit a radiating photon, but still couples strongly to the nanophotonic system via the formation of an atom-photon bound state. The photonic part, unable to propagate, then facilitates tunable and coherent long-range interactions between atoms. Phenomena and applications based upon this effect are discussed in Sec. IV.C.

A. Quantum coherence in a strongly dissipative regime

The intuition behind collective dissipation can be qualitatively understood from Fig. 7(a). In general, a photon emitted

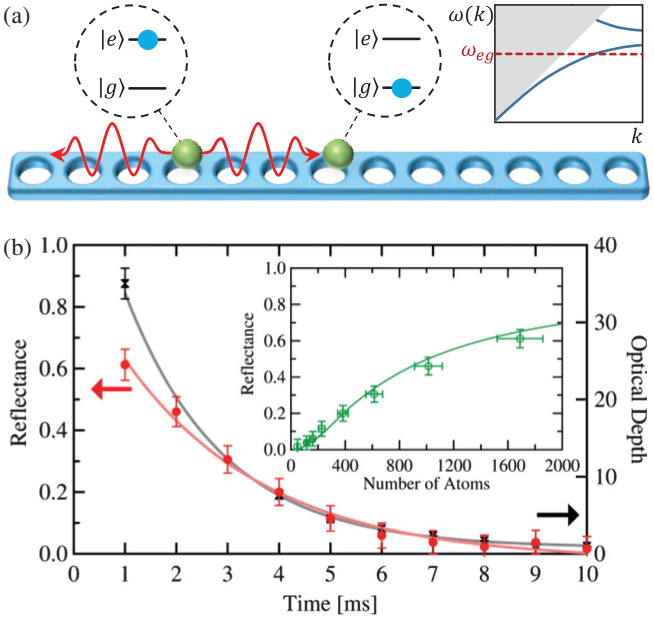

FIG. 7. (a) Atoms coupled to a PCW with the atomic transition frequency ω_{eg} lying within a band of guided modes. Strong quantum coherence effects can emerge from collective dissipation through the waveguide, particularly when atoms are trapped at a spacing equal to integer multiples of half the resonant guided wavelength $\pi/k(\omega_{eg})$, such that the phase factor $e^{ik(\omega_{eg})|z_j-z_l|} = \pm 1$ between any pair of atoms. (b) Experimentally measured reflectance from an atomic ensemble coupled to an optical nanofiber when atoms are trapped near the ideal spacing. The reflectance (red curve) and optical depth (gray) are shown as a function of time. Both quantities decrease in time due to a decrease in the number of atoms (number of atoms shown in the inset). From Corzo *et al.*, 2016.

from atom j acquires a phase factor $e^{ik_0|z_j-z_l|}$ as it propagates to atom l, where $k_0 = k(\omega_{eg})$ represents the guided mode wave vector at the atomic resonant frequency. In the special case that atoms are trapped with lattice constant a equal to the guided mode wavelength itself (i.e., $a = 2\pi/k_0$), the phase factor between any pair of atoms is $e^{2i\pi q} = 1$ (where q is an integer). Thus, incoming fields couple only to a *single*, symmetric and superradiant collective mode of the atoms, whose emission rate into the fiber is enhanced as $N_a\Gamma_{1D}$, while the emission rate of this mode to free space Γ' remains that of a single atom.

While collective enhancement is prevalently used in atomic ensembles (Hammerer, Sørensen, and Polzik, 2010), this manifestation in a 1D waveguide has particularly interesting consequences. For example, the negligible coupling to free space $N\Gamma_{1D} \gg \Gamma'$ implies that the high interaction probability with a resonant guided photon causes it to be coherently *reflected*, rather than being scattered into other directions. Ideally, the fraction of light that is not reflected scales as $\approx 2\Gamma'/N_a\Gamma_{1D}$, indicating that the atomic array acts as a nearly perfect mirror (Chang *et al.*, 2012; Le Kien and Rauschenbeutel, 2014). This effect was recently observed in different experiments (Corzo *et al.*, 2016; Sorensen *et al.*, 2016). Corzo *et al.* (2016) used a near-resonant guided field to trap atoms with a lattice constant near the ideal condition. As

shown in Fig. 7(b), up to 75% reflectance can be seen using merely $N_a \approx 2000$ atoms, which is due to significantly higher OD per atom compared to atomic Bragg mirrors in free space (Deutsch *et al.*, 1995; Andre and Lukin, 2002); see, for example, Birkl *et al.* (1995), Bajcsy, Zibrov, and Lukin (2003), and Schilke *et al.* (2011).

This high reflectance and coupling to the superradiant mode gain additional power with more sophisticated protocols (Chang *et al.*, 2012; Gonzalez-Tudela, Paulisch *et al.*, 2015; Paulisch, Kimble, and Gonzalez-Tudela, 2016; Gonzalez-Tudela *et al.*, 2017). For example, using two atomic ensembles serving as separate "mirrors," one can implement cavity QED protocols, but where the mirrors themselves now have quantum functionality (Chang *et al.*, 2012). It is also possible to coherently manipulate quantum information within the large space of "subradiant" atomic modes that are decoupled from the waveguide and to subsequently map these states out efficiently by transforming to the superradiant mode (Gonzalez-Tudela, Paulisch *et al.*, 2015; Gonzalez-Tudela *et al.*, 2017). Such schemes are discussed in detail in Sec. VII.

B. Chiral quantum optics

A second example of the surprising physics enabled by nanofibers is chiral coupling between atoms and light. For a recent review on this subject, see Lodahl *et al.* (2017). In particular, even if a nanofiber is mirror symmetric, it has been experimentally demonstrated that an excited atom can emit a photon into the waveguide almost purely into just a single direction (Mitsch *et al.*, 2014).

This novel effect arises from the peculiar polarization exhibited by tightly confined optical fields. Specifically, while a plane wave is well known to have a polarization orthogonal to its wave vector (i.e., direction of propagation), a tightly focused beam must necessarily consist of wave vectors that are not purely parallel to its net propagation direction. The beam polarization can thus acquire a component of the electric field along the direction of propagation, which can have $\pi/2$ phase difference with the transversely oriented components (Lin *et al.*, 2013; Rodriguez-Fortuno *et al.*, 2013; Petersen, Volz, and Rauschenbeutel, 2014). Elliptically polarized light is thereby generated in a plane containing the propagation direction and the transverse field. As illustrated in Fig. 8(a) for a nanofiber (Petersen, Volz, and Rauschenbeutel, 2014), the polarization for the electric field external to the fiber can be highly circular with an opposite sense of rotation on opposite sides of the nanofiber. Reversing the propagation direction $z \to -z$ reverses the rotation directions of the field on the two sides of the fiber. This phenomenon is also known as spin-orbit coupling of light.

While the fields in nanofibers and other nanophotonic waveguides satisfy time-reversal invariance (for permeability $\mu = 1$), an atom with nontrivial internal spin structure trapped near these devices can lead to violations of time-reversal invariance for the composite system of waveguide and atom. This means that reversing the direction of propagation of the waveguide modes while keeping the same state in the emitter can lead to nonreciprocal propagation in the forward or backward direction. The first experimental observation of

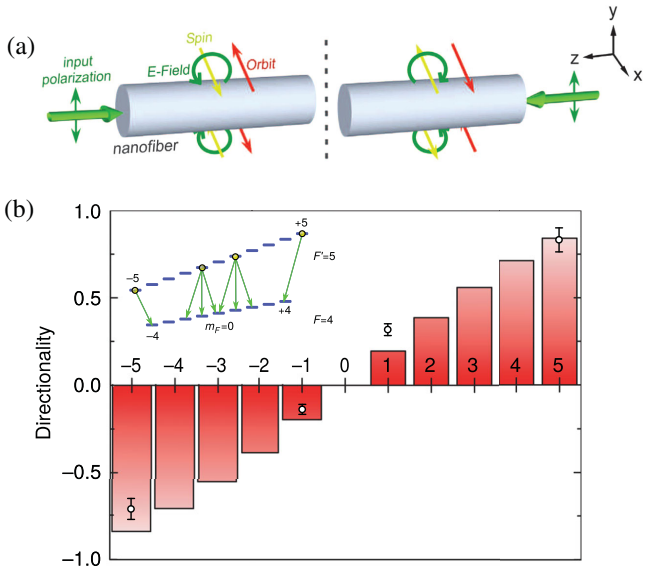

FIG. 8. (a) Interplay between the direction of propagation and polarization of the guided modes of an optical nanofiber, as illustrated in Petersen, Volz, and Rauschenbeutel (2014). A field propagating in one direction can have near circular polarization of different orientations on opposite sides of the fiber. The orientation of circular polarization is reversed in the lab frame for fields propagating in the opposite direction. (b) Measured (circles) and predicted (bars) difference in right- and left-going emitted intensities from different Zeeman levels $m_{F'}$ ($|m_{F'}| \leq 5$ for atomic Cs), normalized by the total guided intensity. From Mitsch *et al.*, 2014.

this effect was reported by Mitsch *et al.* (2014), where through a combination of optical pumping and excitation with well-defined polarization atoms were effectively excited into states of a given Zeeman level $m_{F'}$. For maximum $|m_{F'}|$, the excited atom couples only to σ_+ or σ_- polarization and hence emits light only along $+z$ or $-z$. Figure 8(b) shows the measured and predicted difference in right- and left-going emitted intensities, normalized by the total guided intensity $D = (|E_R|^2 - |E_L|^2)/(|E_R|^2 + |E_L|^2)$ and demonstrates a degree of directionality of $D \approx 0.85$ for the maximum $|m_{F'}|$ states (Mitsch *et al.*, 2014).

The situation where many atoms are coupled to a chiral waveguide, so that each atom only "sees" the emission from other atoms situated to one side, also realizes an interesting class of collective dissipative models, known as a "cascaded" open system (Carmichael, 1993; Gardiner, 1993; Stannigel, Rabl, and Zoller, 2012). Their natural realization in nanophotonic systems has led to novel devices such as nanophotonic optical isolators (Sayrin, Junge *et al.*, 2015). Furthermore, it would allow for the generation of exotic many-body states, provided that the emitted photons are channeled almost completely into the waveguide (Ramos *et al.*, 2014), as discussed further in Sec. VIII.

While the probability of atomic emission into the guided modes of nanofibers is small, $\Gamma_{1D}/\Gamma' < 0.1$ (Mitsch *et al.*, 2014), novel PCW designs coupled to quantum dots have achieved both high yield $\Gamma_{1D}/\Gamma' \gg 1$ and directional β factor $\beta_{\mathrm{dir}} \approx 98\%$ (Sollner *et al.*, 2015), defined as $\beta_{\mathrm{dir}} = \max[\Gamma_R, \Gamma_L]/(\Gamma_R + \Gamma_L + \Gamma')$. Nonreciprocal photon

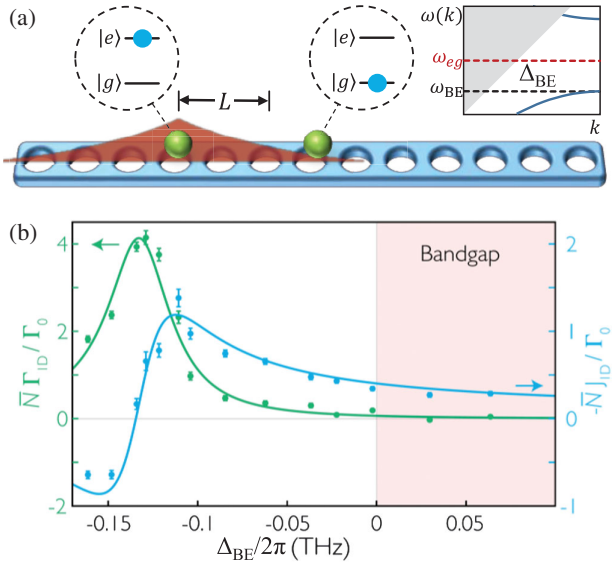

FIG. 9. Quantum many-body physics for atomic transition frequencies in a band gap. (a) Schematic illustration of excited atom and associated photon bound state, with spatial extent L. A second atom nearby in ground state g can be excited by an "exchange" interaction with the first atom. Inset: Band structure with atomic frequency ω_{eg} within a band gap, detuned by Δ_{BE} from the band edge. (b) Measurements showing the collectively enhanced emission rates $\bar{N}_a\Gamma_{1\mathrm{D}}$ (green curve) and coherent interaction strengths $\bar{N}_a J_{1\mathrm{D}}$ (blue curve) near a band edge, both normalized by the vacuum emission rate Γ_0. For detunings $\Delta_{\mathrm{BE}} > 0$, the atomic frequency lies within a band gap, which strongly suppresses emission into the waveguide while coherent interactions persist. Here $\bar{N}_a \simeq 3$ atoms. From Hood *et al.*, 2016.

transport using a Mach-Zehnder interferometer and chiral coupling with quantum dots has also been proposed (Sollner *et al.*, 2015).

Beyond these prospects for chiral quantum optics within the dispersive bands of PCWs, see also Sec. IX.A. There we review possibilities for achieving full quantum control within the band gap of PCWs (as in the following section), including for atom-atom interactions that violate time-reversal symmetry.

C. Quantum many-body physics for atomic spins in a band gap

The enhancement of emission into a preferred channel $\Gamma_{1\mathrm{D}}/\Gamma' \gg 1$ is motivated by the quest to efficiently map between atomic and photonic states. However, there is another regime that has been theoretically considered since the "invention" of photonic crystals, if largely overlooked, which is the behavior of atoms when their transition frequency is situated within a band gap.

Clearly, in this case a single atom cannot emit a propagating photon into the PCW. However, pioneering work in 1990 predicted that ideally, a stable "bound state" could form between an excited atom and a photon, around the atomic position over a length scale L [Fig. 9(a)] (John and Wang, 1990; Kurizki, 1990). These ideas gained renewed interest in recent years, as it was shown that the photonic component of these bound states could enable tunable, long-range interactions between atoms (John and Quang, 1996; Bay, Lambropoulos, and Molmer, 1997; Lambropoulos *et al.*, 2000; Shahmoon and Kurizki, 2013; Douglas *et al.*, 2015; Gonzalez-Tudela, Hung *et al.*, 2015). As illustrated in Fig. 9(a), a second atom initially in its ground state and positioned within the bound-state size of the first excited atom can absorb the photon, thus realizing an effective spin-exchange interaction $|eg\rangle \rightarrow |ge\rangle$ between internal states of the atoms. These coherent interactions can dominate over dissipative mechanisms provided that a high cooperativity is achieved (Douglas *et al.*, 2015; Gonzalez-Tudela, Hung *et al.*, 2015), analogous to the spin-exchange interaction in cavity QED, discussed in Sec. II. Compared to cavity QED, however, PCWs naturally enable interactions of a finite, tunable range (whereas in cavity QED the interaction is naturally infinite range) and with a strength of interaction potentially much greater, owing to the tight confinement of the mediating photon.

An initial experiment to observe signatures of coherent many-body interactions within a band gap was described by Hood *et al.* (2016). Using the APCW structure discussed in Sec. III, the TE-like band-edge frequency (ω_{BE}) was fine-tuned *in situ* to place the atomic transition frequency (ω_{eg}) inside the band gap [i.e., $\Delta_{\mathrm{BE}} = \omega_{eg} - \omega_{\mathrm{BE}} > 0$; see Fig. 9(a)]. For the band-edge detunings Δ_{BE} used in the experiment, the bound photon length L was much larger than the separation between atoms trapped along the APCW. The atomic spins thus effectively interacted through a spin Hamiltonian in the form of Eq. (2) with a uniform peak interaction strength $J_{1\mathrm{D}}$. Inside the band gap, it was observed that $J_{1\mathrm{D}}$ persists even as the dissipative rate $\Gamma_{1\mathrm{D}}$ is exponentially suppressed versus Δ_{BE} [Fig. 9(b)]. A minimum ratio of $\Gamma_{1\mathrm{D}}/J_{1\mathrm{D}} = 0.05 \pm 0.17$ was inferred, in good agreement with theory (Asenjo-Garcia, Hood *et al.*, 2017). In this realization, the free-space emission rate remains comparable to the band-gap-mediated interaction strength $\Gamma' \sim \bar{N}_a J_{1\mathrm{D}}$. Further enhancement of coherent atom-photon coupling (Hood *et al.*, 2016), or suppression on the emission rate Γ' (Hung *et al.*, 2013; Lodahl, Mahmoodian, and Stobbe, 2015), is required to bring such systems into regimes dominated by coherent quantum dynamics.

Taking advantage of the toolbox of quantum optics and the flexible engineering of PCWs, band-gap-mediated interactions allow rather general Hamiltonians of the form $H = \sum_{j,l} U(\mathbf{r}_j, \mathbf{r}_l)\sigma^{(j)}\sigma^{(l)}$ to be realized (Douglas *et al.*, 2015; Gonzalez-Tudela, Hung *et al.*, 2015; Hung *et al.*, 2016). Here $\sigma^{(j)}\sigma^{(l)}$ denotes some type of spin interaction (e.g., XX or Ising) between pairs of atoms j, l, while $U(\mathbf{r}_j, \mathbf{r}_l)$ denotes some interaction of a desired shape and range mediated by the bound photon. The underlying physics will be discussed in greater detail in Sec. IX. This Hamiltonian potentially enables access to a broad range of interesting phenomena. In particular, if the atomic positions are fixed in place, then H describes interactions between spins that can potentially be long range. On the other hand, the positions r_i could be treated as dynamical variables, in which case H describes strong interatomic potentials that depend on the internal atomic state. Finally, the PCW enables efficient spin-photon interactions in that an incoming photon can interact with the atomic internal states with high efficiency. Thus, in total,

aligning atomic transition frequencies within band gaps opens up multiphysics coupling between spins, phonons (atomic motion), and photons. Some specific examples of novel phenomena will be discussed in Secs. X and XI.

D. Coupled cavity arrays

One of the earliest sets of proposals to investigate novel physics using atomic systems and nanophotonics involved the potential for scaling to many atom-cavity systems on a single chip. In particular, whereas a single coupled atom-cavity system is described by the well-known Jaynes-Cummings model, nanophotonics could in principle offer a way to realize a large array, where the cavities are in close enough proximity that photons could "hop" from one to another. Just as the experimental realization of the Bose-Hubbard model with ultracold atoms in optical lattices (Greiner *et al.*, 2002) stimulated intense theoretical and experimental activity with degenerate quantum gases, the question emerged as to whether such a "Jaynes-Cummings-Hubbard" model would be capable of realizing phase transitions or other nontrivial many-body phenomena involving photons (Greentree *et al.*, 2006; Hartmann, Brandao, and Plenio, 2006; Angelakis, Santos, and Bose, 2007). One of the important subtleties of these photonic systems is that they are inherently out of equilibrium, as they require external driving to populate with photons, making theoretical efforts to study such systems correspondingly rich and challenging. The field of many-body physics with photons in coupled cavity arrays already constitutes an active field with a number of thorough reviews (Carusotto and Ciuti, 2013; Noh and Angelakis, 2017), and we direct readers interested in this topic to them. Much of this physics also extends to the microwave domain, where, for example, recently a chain of 72 cavities coupled to superconducting qubits was realized (Fitzpatrick *et al.*, 2017).

V. ATOM-LIGHT INTERACTIONS IN DIELECTRICS: A GREEN'S-FUNCTION-BASED APPROACH

Having qualitatively described some of the physics that can be realized with atoms coupled to nanophotonic systems, we now turn to the important question of how atom-light interactions in these complex optical structures can be rigorously and quantitatively described. Developing fully quantized theories for atom-light interactions in dielectric environments has been a historic open problem in quantum optics. One general strategy relies on finding normal mode decompositions for the field and to subsequently quantize them (Glauber and Lewenstein, 1991; Bhat and Sipe, 2006). This is particularly difficult, however, if the dielectric material itself has losses and dispersion (Bhat and Sipe, 2006) or if the geometry is too complex to solve explicitly for the modes. An alternative approach is to base the quantized description upon the classical electromagnetic Green's function (Agarwal, 1975), a technique formalized in recent years by Welsch and co-workers (Gruner and Welsch, 1996; Knoll, Scheel, and Welsch, 2000; Dung, Knoll, and Welsch, 2002; Wubs, Suttorp, and Lagendijk, 2004; Buhmann and Welsch, 2007). We summarize the main features next, as it has proven to be quite powerful for quantitatively describing atom-nanophotonics interfaces.

Formally, the Green's function represents the electric field at point $\mathbf{r}$ due to a normalized dipole source at $\mathbf{r}'$ and oscillating at frequency ω and is the solution to

$$[(\nabla\times\nabla\times)-\epsilon(\mathbf{r},\omega)\omega^2/c^2]G_{\alpha\beta}(\mathbf{r},\mathbf{r}',\omega)=\delta(\mathbf{r}-\mathbf{r}')\otimes I. \quad (3)$$

Here $\epsilon(\mathbf{r},\omega)$ is the dimensionless electric permittivity, allowed to be position and frequency dependent. $\mathbf{G}$ is a tensor quantity ($\alpha,\beta=x,y,z$), with α denoting the possible polarizations of the field at $\mathbf{r}$ and β the possible source orientations. We refer readers to Buhmann and Welsch (2007) for details of how electrodynamics can be quantized within a Green's function language. However, the essential idea is that in the transition from classical to quantum theory the sources (such as atoms and noise) take on quantum properties, but the fields produced by classical and quantum sources *propagate* in the same way as they both obey Maxwell's equations.

Thus, for a collection of two-level atoms, the quantum field in the Heisenberg picture is intuitively given by (Asenjo-Garcia, Hood *et al.*, 2017)

$$\hat{\mathbf{E}}(\mathbf{r},t)=\hat{\mathbf{E}}_{\rm in}(\mathbf{r},t)+\mu_0\omega_0^2\sum_j\mathbf{G}(\mathbf{r},\mathbf{r}_j,\omega_{eg})\cdot\wp\sigma_{ge}^j(t). \quad (4)$$

This equation simply states that the total field is the sum of the homogeneous solution (the "input," defined absent the atoms but including the dielectric) plus that radiated by the atoms. Such input-output equations were first formally developed within cavity QED (Gardiner and Collett, 1985), allowing the quantum field exiting a cavity to be completely describable in terms of correlations of the atoms and input field alone. Equation (4) can be viewed as a generalization to arbitrary dielectric environments. Just as the calculation of a cavity output field now represents a textbook problem, the power of casting the field generally in this form is that it enables well-developed theoretical approaches to open systems, such as the quantum regression theorem, to be directly applied (Gardiner and Zoller, 2004). What remains then is to describe the dynamics of atoms interacting via the fields. It can be shown that integrating out the field [Eq. (4)] results in an effective master equation describing dipole-dipole interactions $\dot{\rho}=-i[H_{\rm dd},\rho]+L_{\rm dd}[\rho]$, where (Knoll, Scheel, and Welsch, 2000; Asenjo-Garcia, Hood *et al.*, 2017)

$$H_{\rm dd}=-\mu_0\omega_{eg}^2\sum_{j,l}\wp^*\cdot{\rm Re}\mathbf{G}(\mathbf{r}_j,\mathbf{r}_l,\omega_{eg})\cdot\wp\sigma_{eg}^j\sigma_{ge}^l, \quad (5)$$

$$L_{\rm dd}[\rho]=\sum_{j,l}\mu_0\omega_{eg}^2\wp^*\cdot{\rm Im}\mathbf{G}(\mathbf{r}_j,\mathbf{r}_l,\omega_{eg})\cdot\wp \times(2\sigma_{ge}^j\rho\sigma_{eg}^l-\sigma_{eg}^j\sigma_{ge}^l\rho-\rho\sigma_{eg}^j\sigma_{ge}^l). \quad (6)$$

The Hamiltonian $H_{\rm dd}$ describes the coherent exchange of atomic excitations via photons, while $L_{\rm dd}$ describes spontaneous emission. The effective master equation takes an identical form as its free-space counterpart (Lehmberg, 1970). It should also be noted that the spontaneous emission term captures collective effects (Gross and Haroche, 1982) as

it involves correlations $\sigma_{eg}^{j}\sigma_{ge}^{l}$ between different atoms ($j \neq l$). The dependence of the coherent interactions and dissipation on the real and imaginary parts of $\mathbf{G}$ has an elegant classical analogy, in that the field components in and out of phase with an oscillating dipole store time-averaged energy and perform time-averaged work, respectively. We refer to the combination of Eqs. (4), (5), and (6) as the "spin model" of atom-light interactions. We can also group the deterministic part of the evolution ($\sigma_{eg}^{j}\sigma_{ge}^{l}\rho$ and $\rho\sigma_{eg}^{j}\sigma_{ge}^{l}$ terms) of L_{dd} with H_{dd}, such that $\dot{\rho}_{\mathrm{det}} = -i(\tilde{H}_{\mathrm{dd}}\rho - \rho\tilde{H}_{\mathrm{dd}}^{\dagger})$, where $\tilde{H}_{\mathrm{dd}}$ simply contains the full Green's function

$$\tilde{H}_{\mathrm{dd}} = -\mu_0\omega_{eg}^2\sum_{j,l}\wp^* \cdot \mathbf{G}(\mathbf{r}_j, \mathbf{r}_l, \omega_{eg}) \cdot \wp\sigma_{eg}^{j}\sigma_{ge}^{l}. \tag{7}$$

For notational convenience, we often just deal with $\tilde{H}_{\mathrm{dd}}$, with the understanding that the full dynamics involves Eqs. (5) and (6), or alternatively, that evolution under $\tilde{H}_{\mathrm{dd}}$ must be supplemented with stochastic "quantum jumps" to capture the final unaccounted term in $L_{\mathrm{dd}}[\rho]$ (Carmichael, 1993).

The form of Eq. (5) has already appeared implicitly in Sec. II, when we derived the dipole interactions in a Fabry-Perot cavity via the Jaynes-Cummings model, Eq. (2). Intuitively the Green's function in a cavity takes the spatial form $G(\mathbf{r}_j, \mathbf{r}_l, \omega) \propto \cos kx_j \cos kx_l$ as both atoms must be positioned away from a node of the standing wave in order to interact [the equivalence between the Jaynes-Cummings model and the spin model is described in detail by Asenjo-Garcia, Hood *et al.* (2017)]. One also sees from the case of the Jaynes-Cummings model that the spin model is approximate. In particular, $\mathbf{G}$ in the spin model is evaluated only at a single frequency ω_{eg}, which assumes that the dispersion of the dielectric surroundings within the bandwidth of the atomic dynamics is negligible. Consequently, the field in Eq. (4) depends instantaneously on the atomic properties. Within the context of cavity QED, one must then avoid the strong coupling regime $g_{\mathrm{JC}} > |\delta_{\mathrm{JC}}|, \kappa$, where the excited-state population of a single atom can undergo oscillations [whereas Eq. (6) predicts monotonic decay]. Nonetheless, the spin model is valid in a wide variety of scenarios and provides a critical tool for understanding atom-nanophotonics interfaces.

Various elements of the spin model have a long history within atomic physics and quantum optics. For example, in the case of a single atom at position $\mathbf{r}$, the excited-state spontaneous emission rate is given from Eq. (6) by $\Gamma_{\mathrm{tot}} = 2\mu_0\omega_{eg}^2\wp^* \cdot \mathrm{Im}\mathbf{G}(\mathbf{r}, \mathbf{r}, \omega_{eg}) \cdot \wp$. This has long been used to calculate emission rates in simple geometries where the Green's function is exactly solvable, such as near planar surfaces (Agarwal, 1975; Chance, Prock, and Silbey, 2007) and cylindrical nanofibers (Søndergaard and Tromborg, 2001; Klimov and Ducloy, 2004; Le Kien *et al.*, 2005), and is used to evaluate the emission rate near a nanofiber in Fig. 3(d). The Green's function can be numerically evaluated for more complex geometries. For nanophotonic structures, one popular approach is finite-difference time domain (FDTD) (Sullivan, 2013). Here Maxwell's equations are solved on a discrete grid of space and time, and the Green's function can be found by inserting a pointlike source into the simulation. This is a standard technique to evaluate the emission rate of quantum dots and other quantum emitters coupled to nanophotonic cavities and waveguides (Badolato *et al.*, 2005; Manga Rao and Hughes, 2007; Yao, Manga Rao, and Hughes, 2010) and was also used to evaluate the emission rates of atoms near the APCW (Goban *et al.*, 2015) and similar structures (Hung *et al.*, 2013) as shown in Fig. 4(d).

The spin model has also been used to describe various collective atomic phenomena, ranging from superradiant decay (Gross and Haroche, 1982; Araujo *et al.*, 2016) to entanglement generation in photonic structures (Dzsotjan, Sorensen, and Fleischhauer, 2010; Shahmoon and Kurizki, 2013). The idea that field correlations are encoded in atomic correlations was also noticed early on, such as in the theory of single-atom resonance fluorescence (Kimble and Mandel, 1976) or the interference of two-atom emission at close distances (Ficek and Swain, 2002). In later sections, we show that properly combining these various elements constitutes a powerful tool for qualitatively and quantitatively understanding atom-nanophotonics interfaces, even at the many-body limit.

VI. ATOM TRAPPING WITHIN DIELECTRIC NANOSTRUCTURES

Before we present more details on surprising new physics, in this section we take a necessary detour to discuss various schemes to trap arrays of cold atoms within dielectric nanostructures. In Figs. 3(a) and 4(a), we take the artistic license of adding spheres to depict atoms trapped near and interacting strongly with tightly confined, guided fields. Critical to the successful integration of cold atoms with nanophotonics is the development of new trapping techniques and generations of nanophotonic structures that enable these "cartoons" to become reality. These previous and ongoing efforts are aimed at localizing atoms at precisely defined positions, where the atom-photon interactions are optimal. As we will also discuss, one of the big challenges in creating stable traps is the impact of the surface Casimir-Polder force (Casimir and Polder, 1948). The Green's function formalism and numerical methods (both introduced in Sec. V) actually allow us to precisely compute the potential resulting from Casimir-Polder interaction and even design novel surface traps.

A. Overview of optical traps for nanophotonics

In conventional settings in atomic physics, atoms are trapped using optical dipole forces (Grimm, Weidemuller, and Ovchinnikov, 2000). As with dielectric nanoparticles, atoms experience an effective potential due to a spatially inhomogeneous electromagnetic field of frequency ω given by $U(\mathbf{r}) = -\alpha_R(\omega)|\mathbf{E}(\mathbf{r}, \omega)|^2$, where $\alpha_R(\omega)$ is the real part of the (scalar) atomic polarizability (Grimm, Weidemuller, and Ovchinnikov, 2000). For a two-level system, $\alpha_R(\omega)$ is positive (negative) for frequencies ω below (above) the transition frequency ω_{eg}, implying that the atom is attracted toward points of maximum (minimum) intensity. In practice, the field frequency is typically quite different from the resonant frequency, to form a far-off resonant trap (FORT), which suppresses the unwanted effect of motional heating from the recoil momentum kicks associated with scattered photons.

Successful trapping techniques involving nanophotonic systems thus far have utilized two separate strategies. The first employs interference between an external side-illumination field $\mathbf{E}_{\mathrm{SI}}(\mathbf{r},\omega)$ and the reflection of this field from the dielectric $\mathbf{E}_r(\mathbf{r},\omega)$. In this case, it is instructive to consider a dielectric half-space, with $\mathbf{E}_{\mathrm{SI}}$ a plane wave that is normally incident on the dielectric surface from vacuum. The total intensity in the vacuum space is $I(\mathbf{r}) \propto |\mathbf{E}_{\mathrm{SI}}(\mathbf{r}) + \mathbf{E}_r(\mathbf{r})|^2$, which has a field maximum at distance $z_A = \lambda_0/4$ from the dielectric surface, with λ_0 the vacuum wavelength of the side-illumination beam. For "red" detuning $\omega < \omega_{eg}$, atoms can be trapped around this plane of maximum intensity at distance $z_A \sim 200$ nm from the surface of the dielectric.

For a nanoscopic dielectric, the same strategy can be employed, but now with $\mathbf{E}_r(\mathbf{r},\omega)$ calculated numerically and in general varying rapidly around the dielectric surface (Thompson *et al.*, 2013; Goban *et al.*, 2015). An illustration of such a trap is shown in the inset of Fig. 5(a), where a tightly focused beam is reflected from a photonic crystal cavity. In this case the distance to the first interference antinode may be fine-tuned by adjusting the thickness of the illuminated nanostructure, therefore changing the optical phase of the reflected field $\mathbf{E}_r$ relative to $\mathbf{E}_{\mathrm{SI}}$. Tuning the antinode to $z_A < 100$ nm from the surface becomes difficult because of the complex near-field response of the dielectric surfaces and the atom-surface Casimir-Polder interactions.

To date, cold atoms have been successfully loaded into side-illumination traps either stochastically by direct overlapping with a cloud of cold atoms in a MOT (Goban *et al.*, 2015) or deterministically by using the steering optical tweezer method (Thompson *et al.*, 2013) discussed in Sec. III.B. Such a method seems promising in light of separate successful efforts in recent years to load individual atoms into arrays of optical tweezers in free space (Muldoon *et al.*, 2012; Nogrette *et al.*, 2014; Lester *et al.*, 2015; Kim *et al.*, 2016), and to even deterministically realize arrays without "defect" vacancies (Barredo *et al.*, 2016; Endres *et al.*, 2016). Adapting such techniques to the side-illumination scheme could in principle enable ordered arrays of atoms to be trapped near and coupled to nanophotonic structures.

A related solution for transport and trapping with precise control of atomic localization near nanoscale dielectrics is based upon an optical "conveyer" lattice formed by two counterpropagating beams from opposite sides of the dielectric, which are phase coherent but offset in frequency. Atoms can then be coherently transported while trapped in the moving lattice. In this way it becomes possible to place atoms into the vacuum spaces of complex dielectric structures (Gonzalez-Tudela, Hung *et al.*, 2015).

A second distinct strategy for atom trapping is to use the spatially varying guided mode fields of dielectric structures themselves. For trapping external to a waveguide, the evanescent components of one or more guided modes can be combined to achieve stable optical traps (Ovchinnikov, Shul'ga, and Balykin, 1991; Mabuchi and Kimble, 1994). The case of a cylindrical nanofiber is an important example (Dowling and Gea-Banacloche, 1996; Le Kien, Balykin, and Hakuta, 2004). Given that the evanescent field is maximum at the fiber surface, a guided mode that is red detuned ($\omega < \omega_{eg}$) attracts atoms toward the surface, while a blue-detuned beam ($\omega > \omega_{eg}$) repels atoms. As originally proposed by Dowling and Gea-Banacloche (1996) and Le Kien, Balykin, and Hakuta (2004) and realized by Vetsch *et al.* (2010) and Goban *et al.* (2012), a stable trap near the dielectric surface can then be created by a suitable combination of the two, provided that the two beams have sufficiently different wavelengths so that their spatial profiles are not identical.

Because of the relatively simple intensity profile of nanofibers, in such a system optical traps via guided modes necessarily must employ two frequencies and localize atoms in evanescent tails that reduce the interaction probability with near-resonant guided photons. Guided mode optical traps in more complex structures, however, can provide superior dipole coupling between trapped atoms and the electric fields of desired guided modes that facilitate near-resonant atom-photon interactions. Exploiting the design flexibility of PCWs (Hung *et al.*, 2013), for example, stable blue- (red-) detuned FORTs in principle can be formed with just a single propagating mode, whose electric field amplitude of its Bloch wave function $|\mathbf{u}_{k_x}(\mathbf{r})|$ exhibits local minima (maxima) in the vacuum space within the structure. Such guided modes can be found in photonic bands, typically of high order (Hung *et al.*, 2013), with proper mirror symmetries about the principal planes intersecting at the center of a unit cell (the trap center) to offer transverse trapping.

PCWs potentially offer other hybrid approaches to trapping as well, which take advantage of their unique designability. For example, it was proposed that one can combine a guided mode FORT and Casimir-Polder surface attraction to create stable traps in 3D (Hung *et al.*, 2013; Goban *et al.*, 2014). This can be implemented with fundamental guided modes in a simple PCW such as the double-beam structure of Fig. 10(a). Here, a blue-detuned guided FORT provides a periodic set of points with field intensity minima, and thus stable confinement of atoms in the x-y plane of the structure [see Fig. 10(b)]. Cuts of the trapping potential through the trap center along the x and y directions are shown in Figs. 10(d) and 10(e). However, the intensity profile from the trap center out of the plane along z has a local maximum or is at best homogeneous, preventing optical trapping in this direction. The trap becomes closed along this direction only through the inclusion of the surface Casimir-Polder potential, as shown in Figs. 10(c) and 10(f). The calculation of these potentials is discussed in greater detail in the next section. Qualitatively, however, as these forces attract an atom in its ground state toward dielectric surfaces, an atom prefers to sit at $z = 0$ instead of far away from the structure. Of course, this implies that Casimir-Polder forces want to pull atoms away from the symmetry plane $y = 0$ toward one of the dielectric beams, but this effect can be overcome with sufficiently large optical forces. In this particular structure, a modest optical intensity of several $\mathrm{mW\,cm^{-2}}$ is expected to create a deep FORT with >1 mK trap depth along the tightest confining dimension. The Casimir-Polder potential, on the other hand, limits the overall trap depth to $\sim 30\ \mu$K for an atom located at the center of a $g = 250$ nm air gap [Fig. 10(a)].

One advantage of this approach is that additional guided modes supported by the structure can exhibit local electric

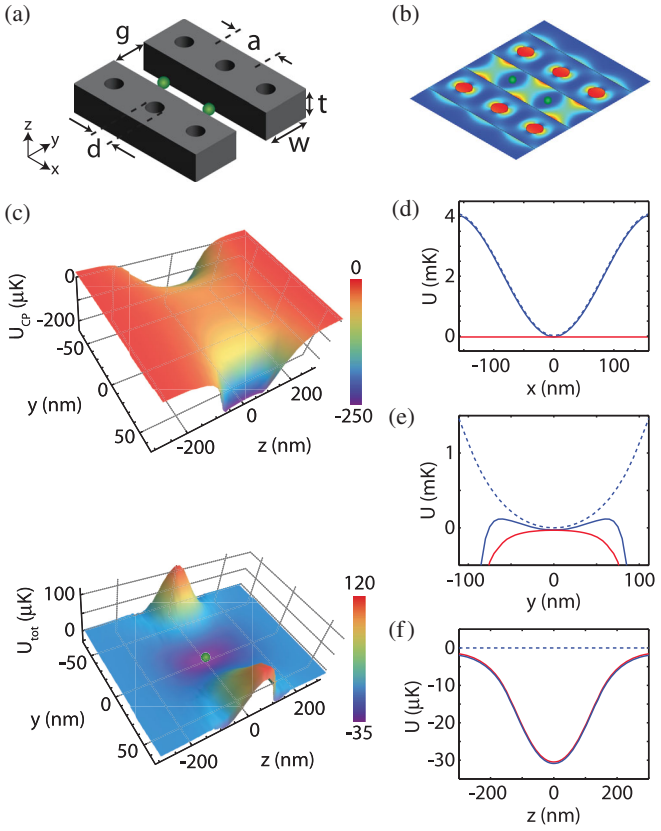

FIG. 10. A hybrid optical and Casimir-Polder trap in a double-beam PCW. (a) Schematic illustration of the waveguide structure. (b) Intensity profile of the blue-detuned guided mode. Green spheres indicate the location of the trap minima. (c) Casimir-Polder potential (top) and the total trap potential (bottom) in the y-z plane. (d)–(f) Line cuts of the Casimir-Polder potential (solid red lines), FORT (dashed blue lines), and total potential (solid blue lines) through the trap center. Adapted from Hung *et al.*, 2013.

field maxima near the trap center, which provides for an increase in interaction probability with near-resonant photons. Trapped atoms in such a system can observe an effective probe mode area as small as $A_{\text{eff}} \sim 0.1\lambda^2$, which is unprecedented in other trapping methods and greatly increases the atom-photon interaction probability. Finally, it should be mentioned that for all of the optical trapping strategies discussed, the internal and external degrees of freedom for trapped atoms can be largely decoupled by using guided modes at "magic" wavelengths for the transition of interest for atom-photon interactions (Ye, Kimble, and Katori, 2008; Goban *et al.*, 2012; Hung *et al.*, 2013).

B. Casimir-Polder potentials

As made clear by Fig. 10, to localize atoms at submicron distances away from structured dielectrics, it is essential to include the effect of Casimir-Polder surface interactions (Casimir and Polder, 1948; Buhmann and Welsch, 2007) into trap calculations. Casimir-Polder interactions arise from an atomic dipole interacting with electromagnetic vacuum fluctuations near structured dielectrics. For ground-state atoms, the Casimir-Polder potential yields strong attraction toward a proximal dielectric surface and can weaken or completely open an otherwise stable FORT potential. To provide a sense of scales, one can consider an atom near a planar dielectric surface, for which an approximate potential (Shimizu, 2001; Friedrich, Jacoby, and Meister, 2002) $V_{\text{CP}}(d) = -C_4/d^3(d + \lambda\!\!\!^{-})$ can be used in place of full QED calculations (Lifshitz, 1956; Agarwal, 1975; Buhmann and Welsch, 2007). Here d is the distance between an atom and the proximal dielectric surface, C_4 is the coefficient for the retarded $1/d^4$ long-range potential, and $\lambda\!\!\!^{-}$ is the effective atomic transition wavelength divided by 2π, a distance below which V_{CP} transitions into $1/d^3$ dependence. For alkali atoms such as rubidium or cesium near silica or silicon-nitride surfaces, $C_4/k_B \sim 5\,\text{nK}\mu\text{m}^4$ and $\lambda\!\!\!^{-} \sim 100$ nm (Friedrich, Jacoby, and Meister, 2002; Bender *et al.*, 2010; Stern, Alton, and Kimble, 2011), resulting in a substantial potential energy variation $\Delta V_{\text{CP}} \sim -k_B \times 250\ \mu\text{K}$ as d changes from 100 to 50 nm.

For complex nanogeometries, analytical calculations for V_{CP} are largely unavailable. Various numerical techniques based on a scattering Green's tensor formalism have been developed to compute Casimir-Polder interactions with general structures; for recent reviews, see Dalvit *et al.* (2011) and Woods *et al.* (2016). Specifically, FDTD (Rodriguez *et al.*, 2009; McCauley *et al.*, 2010) and boundary element (Reid *et al.*, 2009) methods have been implemented to compute atom-nanostructure surface interactions (Hung *et al.*, 2013).

For atomic ground states, the Casimir-Polder interaction can be understood as an energy shift resulting from counter-rotating terms in the full atom-field interaction Hamiltonian, which allows for fluctuations involving the simultaneous creation of a photon and transition to the excited state. As this energy shift of the ground state is position dependent, it can also be interpreted as a motional potential. Excited-state potentials can also be calculated and utilized for atom trapping (Chang *et al.*, 2014), but will not be discussed further here.

Utilizing the fluctuation-dissipation theorem and assuming that the temperature of the nanostructure is much smaller than the atomic transition energies $k_B T \ll \hbar\omega_j$, the ground-state potential can be written as (Buhmann and Welsch, 2007)

$$V_{\text{CP}}(\mathbf{r}) = -\frac{\mu_0\hbar}{2\pi}\text{Im}\int_0^\infty d\omega\omega^2\text{Tr}\{\boldsymbol{\alpha}(\omega)\cdot\mathbf{G}_{\text{sc}}(\omega)\}, \quad (8)$$

where $\mathbf{G}_{\text{sc}}(\omega) \equiv \mathbf{G}(\mathbf{r},\mathbf{r},\omega) - \mathbf{G}_0(\mathbf{r},\mathbf{r},\omega)$ is the difference between the full Green's function at atomic position $\mathbf{r}$ in the presence of the nanostructure and the Green's function $\mathbf{G}_0$ in vacuum. The dynamic polarizability α in Eq. (8) is defined as (Buhmann and Welsch, 2007)

$$\alpha(\omega) \equiv \lim_{\epsilon\to 0}\frac{1}{\hbar}\sum_j \frac{2\omega_j \mathbf{d}_{0j}\mathbf{d}_{j0}}{\omega_j^2 - \omega^2 - i\omega\epsilon}, \quad (9)$$

where ω_j is the transition frequency from the ground state to state j, and $\mathbf{d}_{j0}$ is the corresponding transition dipole moment. In Eq. (8), the integral over frequencies directly reflects the fact that the virtual photon involved in the process can have

any frequency (in contrast to the spontaneous emission rate, for example, where the Green's function is evaluated only at the atomic frequency). Using the property that the Green's function is analytic, in analytical calculations it is often convenient to transform Eq. (8) to an integral over imaginary frequencies (Buhmann and Welsch, 2007) or to an integral over a more general path in the complex plane in the case of numerical calculations (Rodriguez *et al.*, 2009; Hung *et al.*, 2013).

C. 2D vacuum lattices

Apart from representing obstacles to atom trapping via the guided modes of PCWs, Casimir-Polder interactions between an atom and the dielectric environment can be exploited to achieve novel capabilities beyond those possible with either free space or guided optical fields. One example is the creation of 2D "vacuum lattices," where atoms are trapped with a lattice constant much smaller than the free-space wavelength $d \ll \lambda_{eg}/2$. Gonzalez-Tudela, Hung *et al.* (2015) showed theoretically that such vacuum lattices in the x, y plane parallel to the surface of a 2D photonic crystal membrane can yield energy scales for quantum many-body physics (e.g., Bose-Hubbard interactions) roughly 2 orders of magnitude larger than a free-space optical lattice.

The spirit of the idea can already be seen in Contreras-Reyes *et al.* (2010), which calculated the Casimir-Polder interaction of an atom positioned above a 1D dielectric grating made of silicon, as illustrated in Fig. 11(a). The key idea is that a periodic modulation $n(x)$ of refractive index "writes" the same periodicity $V_{\mathrm{CP}}(x,z)$ into the potential. For a sufficiently close distance z_A to the surface (chosen to be $z_A = 300$ nm in the calculation), the modulation in the potential can be significant as illustrated in Fig. 11(b). Importantly, as the periodicity is enforced by that of the underlying dielectric modulation, it is not subject to a minimum "diffraction limit."

In the previous example, the atomic distance z_A to the surface is fixed "by hand," but a scheme for a full 3D trap was proposed by Gonzalez-Tudela, Hung *et al.* (2015) and is schematically illustrated in Fig. 11(c). Here a Rb atom is trapped above a gallium phosphide (GaP) structure consisting of a 2D periodic array of cylindrical posts in a deeply subwavelength regime with lattice constant $d = 50$ nm. In analogy to the previous case, the 2D dielectric modulation creates a 2D lattice arising from the Casimir-Polder potential in the x-y plane. As the potential attracts atoms toward the surface, a fixed distance z_A is maintained by simultaneously illuminating the structure with two counterpropagating side-illumination beams, which provide a stabilizing optical force along z. A cut of the total potential $V_{\mathrm{tot}}(x,y,z_A) = V_{\mathrm{CP}}(x,y,z_A) + V_{\mathrm{SI}}(x,y,z_A)$ along y is shown in Fig. 11(d) at a trapping height of $z_A \approx 32.5$ nm, as is the optical contribution alone. It can be seen that while the optical potential itself is modulated due to scattering from the periodic structure, its modulation depth is weak compared to the dominant Casimir-Polder forces.

The trap depth of this 2D vacuum lattice can be dynamically tuned over a wide range by adjusting the vertical trap position z_A. The trap depth V_d and frequencies ω_{t} for Fig. 11(d) are

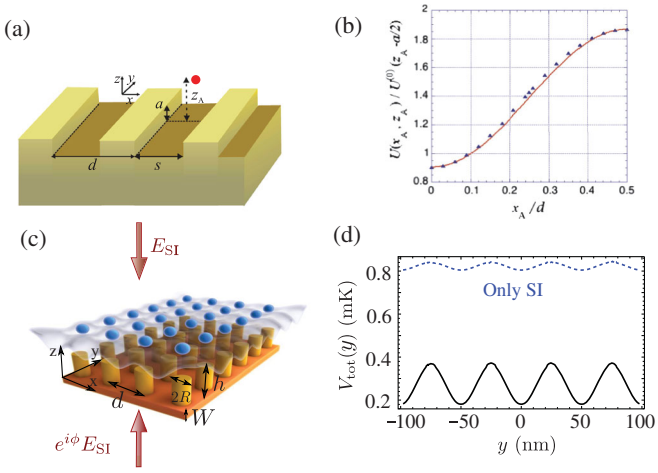

FIG. 11. (a) Schematic of a Rb atom sitting at a fixed distance z_A above a one-dimensional dielectric grating made of silicon. (b) Calculation of Casimir-Polder potential in this geometry along the lateral x direction. The potential $U(x_A, z_A)$ is normalized by the value for a flat interface $U^{(0)}(z_A - a/2)$. The dimensions taken for the calculation are $a = 100$ nm and $d = 2s = 2z_A = 6a$. (a), (b) From Contreras-Reyes *et al.*, 2010. (c) Schematic of a GaP dielectric slab of thickness W with dielectric posts of height h. (d) Cut along y of the total potential (solid black) and side-illumination potential (dotted blue) at $z_A = 32.5$ nm for the case of a ^{87}Rb atom. The chosen dimensions of the structure are $d = 50$ nm, $R = 0.2d$, and $W = h = 119$ nm. (c), (d) From Gonzalez-Tudela, Hung *et al.*, 2015.

$\{V_{d,xy}, V_{d,z}\}/2\pi \approx \{3.5, 20.8\}$ MHz and $\{\omega_{t,xy}, \omega_{t,z}\}/2\pi \approx \{1.7, 4.2\}$ MHz. In the x, y plane, the trapping depth is $\approx 15E_R$, which guarantees the possibility of having localized Wannier modes in the lattice. The side-illumination FORT alone would produce a trap depth of $\approx 3E_R$, which does not lead to localization in a unit cell. The associated photon scattering rate for the chosen parameters is $\approx 2\pi \times 10$ Hz.

VII. COLLECTIVE DISSIPATION

In the remaining sections, we return in more detail to the novel paradigms for atom-light interactions introduced in Sec. IV, beginning here with the manipulation of atomic and quantum optical states via collective dissipation. The key idea is that if a single atom has a significant probability of emitting a photon into a waveguide, then the one-dimensional character of the photonic field guarantees that another atom has a large probability of interacting with the same photon. This quasi-deterministic emission and reabsorption can occur multiple times leading to collective dissipation that can be exploited to obtain interesting many-body states and to trigger multiphoton emission as we will see.

A. Effective description

Let us first consider the simplest paradigm, in which atoms are coupled symmetrically to left- and right-going modes of a broadband 1D waveguide. In such a 1D system and neglecting retardation, a source at z' simply emits a plane

wave $G(z,z') \propto e^{ik(\omega)|z-z'|}$, which following Eq. (7) motivates the following effective Hamiltonian (Dzsotjan, Sorensen, and Fleischhauer, 2010; Gonzalez-Tudela *et al.*, 2011; Chang *et al.*, 2012; Lalumiere *et al.*, 2013):

$$\tilde{H}_{1D} = -i(\Gamma_{1D}/2)\sum_{j,l} e^{ik_0|z_j - z_l|}\sigma_{eg}^{j}\sigma_{ge}^{l} - i(\Gamma'/2)\sum_{j}\sigma_{ee}^{j}. \quad (10)$$

Here $k_0 = k(\omega_{eg})$ represents the propagation wave vector at the atomic resonance frequency. In addition to the atomic interaction mediated by waveguide photons, we have added a phenomenological independent emission rate Γ' of excited atoms into free space. This provides a minimal "toy model" to realistically describe 1D atom-light interfaces, in which the Purcell factor or branching ratio $P_{1D} = \Gamma_{1D}/\Gamma'$ can be considered as the main figure of merit of the system. To connect to an actual specific system, the precise value of P_{1D} and the validity of Eq. (10) can be established by a full numerical or analytical calculation of the Green's function. It is important to note that coupling to radiative waveguide fields results in an intrinsically dissipative Hamiltonian $\tilde{H}_{1D}$. For example, for a single atom $\tilde{H}_{1D} = -(i/2)(\Gamma_{1D} + \Gamma')\sigma_{ee}$ is purely anti-Hermitian and describes excited-state spontaneous emission at a total rate $\Gamma_{1D} + \Gamma'$.

As pointed out in Sec. IV.A, choosing the atomic positions in waveguide QED such that the propagation phase ϕ_{ij} between any two atoms located at z_i, z_j satisfies $\phi_{ij} = |z_i - z_j|k_0 = 2\pi q$ with integer q results in a high probability for photon interaction. In this case, guided mode photons couple to a single collective atomic mode with rate $N_a\Gamma_{1D}$, while atoms emit to free space still with an individual rate Γ'. This situation is described by the effective Hamiltonian

$$\tilde{H}_{1D} \equiv \tilde{H}_{\text{Dicke}} = -i\frac{N_a\Gamma_{1D}}{2}S_{eg}S_{ge} - i\frac{\Gamma'}{2}\sum_{j}\sigma_{ee}^{j}, \quad (11)$$

where

$$S_{\alpha\beta} = \frac{1}{\sqrt{N_a}}\sum_{j}\sigma_{\alpha\beta}^{j}$$

denote collective spin operators. This scenario realizes what is commonly known as the pure Dicke model (Dicke, 1954), a paradigmatic model in quantum optics whose main effects, i.e., superradiance and subradiance (Gross and Haroche, 1982), have remained elusive experimentally in free space due to the complication of additional coherent dipole-dipole interactions in that setting. Waveguide QED allows one to eliminate such detrimental dipole-dipole interactions by precisely positioning the atoms, and furthermore ensures that the superradiant emission goes into the preferred guided modes, as opposed to free space.

The fact that a single collective and superradiant atomic mode couples to the waveguide leads to an interesting linear optical response. In particular, since an incoming guided field couples only to the collective state S_{ge}, and because this state couples with increasing efficiency into the waveguide (at a rate $N_a\Gamma_{1D}$ vs Γ' into free space) with increasing N_a, the system becomes increasingly one dimensional in its response to light. Specifically, a near-resonant photon is unlikely to be scattered into free space but is instead coherently reflected. Using the input-output equation (4), it can be shown that on resonance the fraction of intensity reflected is given by $(N_a\Gamma_{1D})^2/(N_a\Gamma_{1D} + \Gamma')^2$.

This system also reveals interesting characteristics beyond its linear response (i.e., the single-excitation manifold). An important characteristic of the Dicke model is that all symmetric states of N atoms containing m excitations (the so-called Dicke states $|E_m\rangle \propto \text{sym}\{|g\rangle^{N-m} \otimes |e\rangle^{m}\}$) decay with an enhanced rate due to the presence of the other atoms, namely, $\Gamma_{E_m} \approx mN$ for $m \ll N$, which is the limit of interest here. On the other hand, the states satisfying $S_{ge}|\Psi\rangle = 0$ are dark (subradiant) with respect to the collective dissipation induced by the waveguide and comprise the so-called decoherence-free subspace (Zanardi and Rasetti, 1997; Lidar, Chuang, and Whaley, 1998), and have lifetimes limited only by residual free-space emission Γ'. Intuitively, these states are odd with respect to permutation of particles, which causes emission into the waveguide to cancel. For example, for $N = 2$ there is only a single dark state with one excitation given by $(|eg\rangle - |ge\rangle)/\sqrt{2}$.

B. Dynamics within decoherence-free subspaces

These subradiant states cannot be directly probed by the waveguide modes because they are decoupled from them. However, when a weak perturbation provided by an external laser is applied to the system (with a corresponding Hamiltonian $\|H_L\| \ll \Gamma_{1D}$), the collective dissipation of the waveguide projects the dynamics from H_L into the decoherence-free subspaces due to the so-called *quantum Zeno effect* (Misra and Sudarshan, 1977; Beige *et al.*, 2000; Facchi and Pascazio, 2002). This effect gives rise to an effective Hamiltonian $H_{L,\text{eff}} = \mathcal{P}_{\text{DFS}}H_L\mathcal{P}_{\text{DFS}}$ that connects to first order in $||H_L||/\Gamma_{1D}$ only the states within the decoherence-free subspaces and which allows one to obtain interesting many-body states without being affected by the collective dissipation of the waveguide.

To illustrate how we can move within decoherence-free subspaces exploiting quantum Zeno dynamics, we start with a simple example as depicted in Fig. 12(a). Let us consider two two-level atoms strongly coupled to a waveguide in the Dicke regime. In this case, the effect of the interaction of the waveguide is to renormalize the decay rates of the different states. Namely, the symmetric combination of excitations $|ee\rangle$ and $|+\rangle = (|eg\rangle + |ge\rangle)/\sqrt{2}$ experience an enhanced decay of $2\Gamma_{1D}$, whereas the antisymmetric one $|-\rangle = (|eg\rangle - |ge\rangle)/\sqrt{2}$ and $|gg\rangle$ are decoupled from the waveguide. Hence, when we address the two atoms with lasers with Rabi frequencies $|\Omega_{1,2}| \ll 2\Gamma_{1D}$, all the population in states coupled to the waveguide will quickly decay into $|gg\rangle$. The dynamics is thus projected only into the decoherence-free states giving rise to a unitary dynamics within this subspace:

$$H_{L,\text{eff}} \approx \left(\frac{\Omega_1 - \Omega_2}{\sqrt{2}}|gg\rangle\langle -| + \text{H.c.}\right).$$

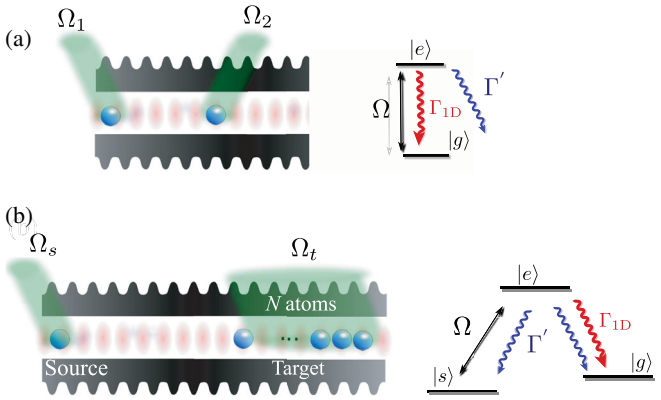

FIG. 12. (a) Schematic of two two-level atoms coupled to a waveguide and individually addressed by lasers $\Omega_{1,2}$. The single-atom level structure consists of atomic ground and excited states $|g,e\rangle$, where $|e\rangle$ decays into the waveguide and free space with rates Γ_{1D} and Γ', respectively. (b) Scheme for quantum state engineering: one single atom is separated several wavelengths apart such that it can be individually addressed with respect to an atomic ensemble of N atoms that is collectively driven.

By choosing an appropriate pulse timing or amplitude for the locally applied lasers, one can prepare the entangled state $|-\rangle$ from an unentangled one $|gg\rangle$. Notice that by performing a local phase change, one can execute the transformation $|-\rangle \to |+\rangle$, which subsequently triggers the emission of a single photon into the waveguide $|+\rangle \to |gg\rangle|1_{wg}\rangle$. The same argument holds for $N_a > 2$ with the advantage that the dimension of the decoherence-free subspaces grows exponentially with N_a and allows one to have subradiant states with more than one excitation. For example, with $N_a = 4$ six subradiant states emerge, three sharing a single excitation and three with two excitations. Using these states one can encode two logical qubits and define a universal set of quantum gates to build more complex states (Paulisch, Kimble, and Gonzalez-Tudela, 2016), which can be used to trigger the emission of two-photon states.

An intriguing question is whether this idea can be extended with increasing N_a to move around in a dark-state subspace and finally generate an arbitrary photon Fock state or superposition of Fock states. Using only two-level systems, the complexity of the Hilbert space makes it difficult to go to large numbers of excitation or photons. Fortunately, the possibility of having several metastable states and optical transitions allows one to define a set of states where this can be readily accomplished. In particular, we now consider a Λ level structure as depicted in Fig. 12(b) in which one optical transition $|e\rangle \leftrightarrow |g\rangle$ couples to the waveguide with rate Γ_{1D}, whereas the other one $|e\rangle \leftrightarrow |s\rangle$ couples to a classical field with Rabi frequency Ω_n.

Consider the superposition state $|\psi_m\rangle = \sum_{p=0}^{m} d_p |S_p\rangle$ for N_a atoms sharing up to m excitations, where the metastable states $|S_m\rangle \propto \mathrm{sym}\{|g\rangle^{N_a-m}|s\rangle^m\}$. It can be shown that $|\psi_m\rangle$ can be efficiently mapped to multiphoton states (Porras and Cirac, 2008; Gonzalez-Tudela, Paulisch *et al.*, 2015) by performing a fast π pulse with $\Omega_n \gg \Gamma_{1D}$ such that $|S_m\rangle \to |E_m\rangle \to (A_{k_0}^\dagger)^m|m\rangle \otimes |g\rangle^{N_a}$, where $|E_m\rangle$ are the Dicke states defined in the previous section. This state rapidly decays to the atomic state $|g\rangle^{N_a}$, while simultaneously emitting a single-mode photon pulse described by A_{k_0} into the waveguide, with a very favorable error scaling as $\propto 1/N_a P_{1D}$ due to superradiant effects.

Of course, the generation of the entangled atomic state $|S_m\rangle$ with a fixed excitation number m is difficult in conventional settings because an atomic ensemble with many atoms behaves like a linear system. However, Gonzalez-Tudela, Paulisch *et al.* (2015) showed that one can exploit atom-waveguide QED characteristics to generate $|S_m\rangle$ by using a configuration as shown in Fig. 12(b). Here a source atom is placed far from the atomic target ensemble in which we want to generate $|S_m\rangle$. Although remotely located, the source atom is still strongly coupled to the same waveguide mode as the target ensemble. Starting with the source atom in $|s\rangle$, and the atomic ensemble in $|g\rangle^{N_a}$, one can exploit quantum Zeno dynamics to transfer the spin excitation $|s\rangle$ collectively to the target ensemble only using subradiant states. By reinitializing the source atom and repeating this process M times, one can indeed obtain any arbitrary superposition $\sum_{m=0}^{M} d_m |S_m\rangle$ in the ensemble, which can be reversibly mapped to photons to generate an arbitrary superposition in the output photon field.

For completeness, let us mention that in both the two-level and the Λ configurations there are two main sources of errors, which arise from the decay of subradiant states to free space through Γ' and from the small populations of superradiant states (which scale with $\propto |\Omega|^2/\Gamma_{1D}$). These two sources give rise to an error in photon state generation $\propto 1/\sqrt{P_{1D}}$, similar to other quantum information protocols in cavity QED (Beige, Braun, and Knight, 2000). By using extra auxiliary atoms and heralding measurements exploiting the high-collection efficiency of the waveguide photons, one can considerably improve the error scaling (e.g., error $\propto 1/N_a P_{1D}$) at the expense of making the process probabilistic (Gonzalez-Tudela *et al.*, 2017).

VIII. SPIN-ORBIT COUPLING OF LIGHT

While the previous toy-model description of an atom-waveguide setup through $\tilde{H}_{1D}$ is reasonable for many situations, it neglects the vector nature of the electromagnetic field and thus the unique polarization properties that tightly guided modes can have. As discussed in Secs. III and VI, the local polarization of the fields of nanostructures can become connected to the direction of propagation of light, leading to *chiral* light-matter interactions [see Lodahl *et al.* (2017) for a review on the subject]. With appropriate design, it then becomes possible to separately tailor the atomic emission into right- and left-propagating modes.

A. Effective description for a chiral setup

A minimal description for chiral coupling assumes that an optical transition $|g\rangle$-$|e\rangle$ of a single atom emits into the left- and right-propagating modes at rates $\Gamma_{L/R}$, respectively. The guided modes in each direction can be adiabatically eliminated, leading to a cascaded quantum system (Carmichael, 1993; Gardiner, 1993; Pichler *et al.*, 2015) whose effective

Hamiltonians $\tilde{H}_{L/R}$ describe dynamics in which atoms interact only with atoms to the right or left (Ramos *et al.*, 2014; Pichler *et al.*, 2015):

$$\tilde{H}_{L/R} = -i\frac{\Gamma_{L/R}}{2}\sum_{j>l/j<l}(e^{ik_0|z_j-z_l|}\sigma_{eg}^{j}\sigma_{ge}^{l} - \text{H.c.}) - i\frac{\Gamma'}{2}\sum_{j}\sigma_{ee}^{j}. \tag{12}$$

Again, we added a phenomenological independent decay rate Γ' to describe free-space emission. One can define two figures of merit $\beta_{L/R} = \Gamma_{L/R}/(\Gamma_L + \Gamma_R + \Gamma')$, which characterize the amount of left or right emission compared to the total one. In the extreme case where $\beta_{R/L} = 1$ (and $\beta_{L/R} = 0$), the atoms see the rest of the atoms only on their right or left, due to the ordering $j > l$ or $j < l$ appearing in the sum of Eq. (12). The bidirectional situation is recovered by setting $\Gamma_R = \Gamma_L = \Gamma_{1D}/2$.

B. Nonreciprocal photon transport

In the bidirectional situation described in Sec. VII, a photon propagating in the left or right direction will scatter in the same way with an atom independent of the direction of propagation, e.g., it will be perfectly reflected in the case $\Gamma' = 0$. In the chiral configuration, even for $\Gamma' = 0$, the right or left transmission and reflection coefficients are given by

$$t_{R/L} = 1 - 2\beta_{R/L}, \tag{13}$$

$$r_{R/L} = -2\sqrt{\beta_R\beta_L}, \tag{14}$$

and thus the system can exhibit an asymmetric optical response if $\beta_R \neq \beta_L$, without the need of using magneto-optical materials. This asymmetry was exploited by Sayrin, Junge *et al.* (2015) for an optical nanofiber to achieve nonreciprocal photon transport with both atomic ensembles and single atoms with a V-type level structure. The idea is to use a magnetic field such that one optical transition couples resonantly with right-moving photons with right circular polarization, while making off-resonant linear and left-circularly polarized atomic transitions as shown in the inset of Fig. 8(b). Hence, when a photon propagates right (left) there is a strong (weak) interaction with the emitter, enabling a demonstration of $\beta_R/\beta_L = 11.5$ for the optical transition of interest. In order to increase the probability of interaction, they used either an atomic ensemble with $N \approx 27$ atoms or a whispering-gallery-mode resonator, being able to obtain experimental isolations of 7.8 and 9.1 dB, respectively, while maintaining high forward transmission.

Sayrin, Junge *et al.* (2015) scattered away a "blocked" photon incoherently. While this functions as a classical optical isolator, for quantum applications it would instead be desirable to realize a unitary nonreciprocal device, which preserves the quantum properties of the input and output channels. Such a scheme was proposed by Sollner *et al.* (2015). Here a single quantum emitter is placed into one arm of an interferometer, and a π shift associated with chiral transmission is then used to route photons coherently depending on their direction of propagation. This would enable one to create coherent superpositions of having been routed or not.

C. Many-body entangled steady states

Instead of probing the atomic system through few-photon scattering, an interesting alternative consists of driving the emitters with classical fields (Ficek and Tanas, 2002), such as external fields transverse to the waveguide or through the waveguide with an auxiliary (nonchiral) guided mode. In that case, one might expect interesting steady states to emerge resulting from the interplay between the chiral collective dissipation and driving. The driving is described by an additional Hamiltonian:

$$\tilde{H}_S + H_{\text{las}} = \sum_j \delta_j \sigma_{ee}^{j} + \sum_j \Omega_j(\sigma_{eg}^{j} + \sigma_{ge}^{j}), \tag{15}$$

where $\delta_j = \omega_{eg} - \omega_L$ is the detuning between the atomic and laser frequencies. For a bidirectional waveguide, steady-state entanglement was predicted by driving the atoms resonantly $\delta_j = 0$ (Gonzalez-Tudela *et al.*, 2011; Gonzalez-Tudela and Porras, 2013). However, the resulting state was mixed and therefore not maximally entangled. Recently, in a series of works (Ramos *et al.*, 2014; Pichler *et al.*, 2015) it was shown that chiral light-matter couplings together with suitable optical detuning patterns $\{\delta_j\}$ can give rise to pure many-body entangled states. To provide a simple illustration of this effect, we consider just two atoms and choose $\Omega_1 = \Omega_2 \equiv \Omega$ and $\delta_1 = -\delta_2 \equiv \delta$. In the idealized limit where $\Gamma' = 0$, it can readily be verified that there exists a dark state $|D\rangle$, which is an eigenstate of the total (non-Hermitian) effective Hamiltonian with zero decay rate into the waveguide. This state is given by

$$|D\rangle = \frac{1}{\sqrt{1+|\alpha|^2}}(|gg\rangle + \alpha|-\rangle), \tag{16}$$

where $|-\rangle$ is a singlet state of the two atoms. Being the unique dark state, the system is deterministically driven to $|D\rangle$ as the steady state. The parameter $\alpha = -2\sqrt{2}\Omega/[2\delta + i(\Gamma_R - \Gamma_L)]$ gives the singlet fraction and can be controlled through either the laser amplitude and/or detuning. The situation for systems $N > 2$ is more intricate as different nonequivalent dark states may appear. On the one hand, there is a trivial generalization of the $N = 2$ case in which the atoms form singlets in pairs. On the other hand, by choosing the detuning pattern appropriately, k-particle entangled states can emerge, which cannot be obtained using only bidirectional waveguides.

IX. BAND-GAP PHYSICS

In Secs. VII and VIII we described the prospects for utilizing collective dissipation, associated with large and possibly directional emission rates into a waveguide, to realize interesting quantum states of matter and light. On the other hand, it would be highly desirable to realize purely coherent dynamics as well, with a strength that is large relative to the emission rate Γ' into free space, but where dissipation due to emission of photons into the waveguide is switched off. It is

helpful to recognize that this dissipation results from the continuum of guided modes at the atomic resonance frequency, and thus a tantalizing "fix" is to shift the atomic frequency away from the propagating modes of a PCW band edge and into the band gap. We now discuss this scenario in this section.

Theoretical investigations of atom-light interactions within a band gap began not long after the "discovery" of photonic crystals (John and Wang, 1990, 1991; Kurizki, 1990; Bay, Lambropoulos, and Molmer, 1997; Lambropoulos *et al.*, 2000). Formally, the typical approach was to consider a hypothetical set of photon modes k (an index for wave vector, for example) described by annihilation operators $\hat{a}_k$, which couple to an atom at position r, $H_{\text{band}} = \hbar\sum_k \omega_k a_k^\dagger a_k + \hbar\omega_{eg}\sigma_{ee} + \hbar\sum_k (a_k e^{ik\cdot r}\sigma_{eg} + \text{H.c.})$. If one chooses a simple gapped dispersion relation, such as $\omega(k) = \omega_{\text{BE}}[1 - \alpha(k/k_b)^2]$ (where $\omega_{\text{BE}} < \omega_{ge}$, so that the atomic frequency lies within the band gap), then the single-excitation manifold is exactly solvable. One of the surprising features is the emergence of an eigenstate $|\psi_b\rangle = \cos\theta|e,0\rangle + \sin\theta|g,1\rangle$ that is a superposition of an excited atom and a photon localized around the atomic position, i.e., an atom-photon bound state (John and Wang, 1990); see Fig. 9(a). Qualitatively, the dressing of an excited atom by a localized photon enables this excitation to hop to nearby atoms, thus realizing an effective spin-exchange interaction. The corresponding effective Hamiltonian for the atoms would then be purely coherent and dissipation free as already noted in many works (Kurizki, 1990; John and Wang, 1991; Bay, Lambropoulos, and Molmer, 1997; Lambropoulos *et al.*, 2000; Shahmoon and Kurizki, 2013).

As these works considered highly idealized dispersion relations, it was not possible to account for "real" systems, which not only see the gapped guided modes of the PCW but free-space modes as well (and thus a dissipation Γ'). The effects of free-space emission, photon decay, band structure, and electric field profiles for realistic PCWs in 1D and 2D were added to such simple models in Douglas *et al.* (2015) and Gonzalez-Tudela, Hung *et al.* (2015). Significantly, it was shown that for 1D waveguides, an intuitive, effective model could achieve good quantitative agreement with numerical simulations of the full Green's function (Douglas *et al.*, 2015).

We thus present the effective model here, which is already suggested by the form of the eigenstate $|\psi_b\rangle$. In particular, this eigenstate looks identical in form to one of the dressed eigenstates $|\psi_+\rangle$ of the Jaynes-Cummings model (see Sec. II). This mapping can in fact be made formal—the photon confined around the atom has the same functionality as the mode of an actual cavity. The effective vacuum-Rabi splitting g_{JC} is identical to that of a real cavity whose mode volume is the same as the bound photon size $V_{\text{eff}} = A_{\text{eff}}L$, where A_{eff} and L are the transverse mode areas associated with the PCW and the bound state length [Fig. 9(a)], respectively. The effective atom-cavity detuning $\delta_{\text{JC}} = 2\Delta_{\text{BE}} = 2(\omega_{eg} - \omega_{\text{BE}})$ is twice the detuning between the atomic frequency and the band edge. The length L itself is in principle tunable, as it is dictated by the detuning from the band edge and the band curvature $L = \sqrt{\alpha\omega_{\text{BE}}/k_b^2\Delta_{\text{BE}}}$. Thus, for example, a more localized photon arises with larger detuning Δ_{BE} or flatter bands.

Utilizing this mapping to cavity QED, one can then immediately conclude that an effective spin interaction such as Eq. (2) is possible using the PCW, except that now the spatial range reflects the shape of the localized photonic cloud:

$$H_{\text{bg}} = (\hbar g_{\text{JC}}^2/\delta_{\text{JC}})\sum_{j,l} e^{-|z_j - z_l|/L} u(z_j)u(z_l)\sigma_{eg}^j\sigma_{ge}^l. \tag{17}$$

Here the exponential envelope results from the localization of the bound photon, while $u(z)$ is a periodic function associated with the shape of the Bloch modes around the band edge [in generic structures, $u(z) = \cos kz$ has the same sinusoidal modulation as a Fabry-Perot cavity, see Fig. 4(c)]. Alternatively, in the language of the spin model this interaction arises from the Green's function $G(z,z') \propto e^{-|z-z'|/L}$ in the band gap.

Finally, the cavity QED mapping enables one to qualitatively understand the role of dissipation. As in our analysis of two atoms in the Jaynes-Cummings model, two atoms interacting via a band gap would be able to exchange a spin excitation with a minimum error of $\mathcal{E} \propto 1/\sqrt{C}$, where $C = \lambda_{eg}^3 Q/V_{\text{eff}}$ depends on the quality factor of the localized photon and its confinement. One can explicitly separate out the photon length dependence $C = C_\lambda(\lambda_{eg}/L)$, where C_λ represents the cooperativity for a photon confined to a length $L = \lambda_{eg}$. The quality factor Q of the bound photon, defined as the ratio of its frequency and decay rate $Q = \omega_{eg}/\kappa$, is limited by absorption and scattering from defects in the PCW and thus far has not been directly measured. However, one would intuitively expect a similar decay rate κ as can be achieved in an actual photonic crystal cavity made from the same material and fabrication processes. The projected cooperativities of $C_\lambda \sim 10^4$ point to the potential to realize coherent interactions with a highly tunable range, which is not readily achievable using other interaction mechanisms.

The same concepts discussed for one-dimensional PCWs also extend to two-dimensional structures with atomic transition frequencies in a band gap. Assuming an isotropic dispersion around the edge of the band, the resulting envelope of the atom-atom interactions scales as (Gonzalez-Tudela, Hung *et al.*, 2015) $f_{2\text{D}}(z_j, z_l) \propto K_0(|z_j - z_l|/L)$, where $K_0(x)$ is the Hankel function. This function in turn scales as $K_0(x) \sim e^{-x}/\sqrt{x}$ and $\log(1/x)$ when $x \ll 1$ and $x \gg 1$, respectively. The overall coupling strength g_{JC} is again set by the effective mode volume, which now scales as $V_{\text{eff}} = L^2 L_{\text{eff}}$. Here L is the linear extent of the photon bound state in the 2D plane, while L_{eff} represents the out-of-plane confinement length. Likewise, the mode volume also dictates the effective cooperativity. In 2D one obtains a scaling of $C_{2\text{D}} = C_\lambda(\lambda/L)^2$, such that $C_{2\text{D}} \geq 100$ over an interaction length of $L \lesssim 10\lambda_{eg}$. However, as the interaction extends now over a plane, the number of atoms that could be coupled while maintaining such $C_{2\text{D}}$ will be similar as for the 1D case.

A. Designing band-gap interactions with the atomic physics toolbox

The natural form of the band-gap-mediated interactions between atoms is to decay exponentially with atomic

separation. In the thermodynamic limit, as the system size approaches infinity, these interactions are designated as short ranged. However, in practice the decay length can be on the same scale as the length of the PCW itself and can thus effectively appear long ranged. Long-range interacting spin systems have been of great interest recently. For example, quantum correlations propagate at a distinctly different speed in the presence of long-range interactions, i.e., for power law decay $1/r^{\alpha}$ with α smaller than the system dimensionality (Hauke and Tagliacozzo, 2013; Schachenmayer *et al.*, 2013; Gong *et al.*, 2014; Jurcevic *et al.*, 2014; Richerme *et al.*, 2014). One limitation to investigations of such physics within the context of photonic crystals is that for two-level systems the type of spin interaction (of exchange type) is fixed, as is the interaction range L for a given structure design, unless the structure itself exhibits some dynamic tunability [for example, via piezoeletric strain (Wong *et al.*, 2004) or optomechanical forces (Rosenberg, Lin, and Painter, 2009)]. In addition, a typical excited state Γ' decays on a scale that would make measurements difficult. We discuss how these issues can be circumvented using the toolbox of atomic physics.

1. Dynamically shaping interactions with Raman lasers

One possible approach is to exploit multilevel atomic structure. For example, dynamical control of the couplings can be achieved by using an atomic Λ transition as depicted in Fig. 13(a), where the excited state apart from being coupled through the waveguide to $|g\rangle$, is off-resonantly driven with detuning δ_L by a Raman laser with Rabi frequency Ω from another auxiliary metastable state $|s\rangle$ (Douglas *et al.*, 2015; Gonzalez-Tudela, Hung *et al.*, 2015). When $|\delta_L| \gg |\Omega|$, the excited state can be adiabatically eliminated giving rise to an XY interaction between the effective spin system defined by $\{|g\rangle, |s\rangle\}$, i.e.,

$$H_{XY} = \hbar \frac{\bar{g}_{\mathrm{JC}}^2}{\Delta_L} \sum_{j,l}^{N} \sigma_{sg}^{j} \sigma_{gs}^{l} f(z_j, z_l). \tag{18}$$

The coupling strength is reduced by the Raman factor $\bar{g}_{\mathrm{JC}} = g_{\mathrm{JC}}(\Omega/\delta_L)$, while the virtual excited-state population scales as $(\Omega/\delta_L)^2$, thereby leading to the same cooperativity as in the two-level case. Importantly, the effective detuning $\Delta_L = \omega_{eg} - \delta_L - \omega_{\mathrm{BE}}$ (see Fig. 13) from the band edge can be dynamically changed by adjusting the frequency of the Raman laser. This configuration has considerable advantages as follows: (i) the spin systems are defined in metastable states and are therefore long lived; (ii) the interaction can be turned on or off at will via a time-dependent $\Omega(t)$, which is very useful to freeze the dynamics at a certain time for measurement; and (iii) the interaction range $L \propto 1/\sqrt{\Delta_L}$ may be dynamically tuned for a fixed nanostructure such that one does not have to rely completely on nanoengineering.

Moreover, Douglas *et al.* (2015) showed that if several Raman lasers are used with different detunings, the interaction obtained between them is a combination of exponentials with different lengths as the adiabatic elimination of fields is additive, such that $f(z_j, z_l) = \sum_{\beta} e^{-|z_j - z_l|/L_\beta} \sim 1/|z_j - z_l|^{\alpha}$ can mimic power law decays over a finite-size system. It is also possible to realize other types of spin interactions, such as Ising, by using different laser configurations or level structures (Douglas *et al.*, 2015; Gonzalez-Tudela, Hung *et al.*, 2015).

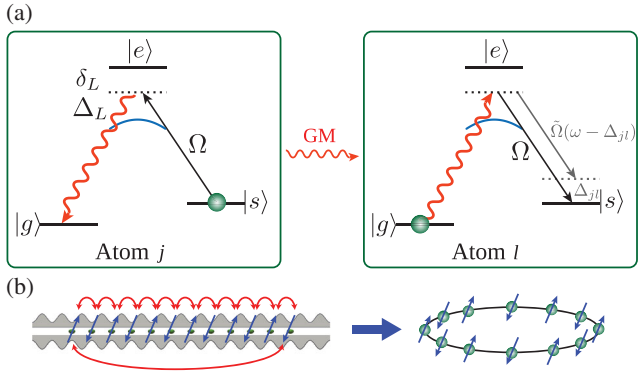

FIG. 13. (a) Dynamical control of atom-atom interactions using a Λ atomic level scheme. The transition $|g\rangle$-$|e\rangle$ is coupled to the modes of the PCW, while the transition $|s\rangle$-$|e\rangle$ is off-resonantly driven (detuning δ_L) by an external laser Ω. Atoms j and l may then exchange excitations in level s via the illustrated two-photon processes. When this exchange occurs within the band gap, the detuning Δ_L from the band edge (blue curve) tunes the range of the effective spin-exchange interaction. Furthermore, for full control of atom-atom interactions, arbitrary long-range spin-exchange interaction between atoms j and l may be engineered. In particular, a relative shift of the s level of atom l by Δ_{jl} matched by a sideband of the Raman laser $\tilde{\Omega}$ (shown in gray), selectively creates an interaction between these two atoms. (b) By engineering the interactions (red arrows mark nearest-neighbor interactions) between the atoms at each end of a finite linear chain using this full control technique, the system can be mapped to a chain with periodic boundary conditions.

2. Full control of spin interactions

Beyond the functional forms derived from the multilevel control schemes, it is possible using magnetic fields to fully control the spin interactions. As illustrated in Fig. 13(a), by applying a magnetic-field gradient, relative, spatially dependent shifts Δ_{jl} of the metastable state s are created between atoms j and l (Hung *et al.*, 2016). Spin interactions can then be engineered selectively between pairs of atoms by introducing sidebands in the Raman control laser Ω that match these shifts. It is thereby possible to engineer a Hamiltonian with pairwise tunable, long-range spin interactions

$$H_{XY,\mathrm{full}} = \hbar \sum_{j,l} J_{jl} \sigma_{sg}^{j} \sigma_{gs}^{l}, \tag{19}$$

where the amplitude and phase of the coupling amplitudes J_{jl} are determined by external fields $\Omega(t) = \sum_{\alpha} \tilde{\Omega}_{\alpha} e^{i\omega_{\alpha} t}$. Through a global rotation of the spin basis, pairwise ZZ interactions can also be engineered stroboscopically.

This highly tunable platform opens a number of avenues for exploration. For example, full control of spin interactions allows for the investigation of frustrated magnetism with long-range interactions or the engineering of periodic boundary conditions, e.g., to realize the Haldane-Shastry spin chain as

shown in Fig. 13(b). Similar to the Raman-addressing schemes already developed in cold atoms and trapped ions (Jaksch and Zoller, 2003; Bermudez, Schaetz, and Porras, 2011; Kolovsky, 2011; Aidelsburger *et al.*, 2013; Miyake *et al.*, 2013), here the interaction coefficients J_{jl} can also acquire a complex phase $J_{jl} = |J_{jl}|e^{i\phi_{jl}}$ by properly arranging the propagation phases of the Raman sidebands. This allows the engineering of geometric phases in the spin model that mimic the effect of strong magnetic fields acting on charged particles, thereby breaking time-reversal symmetry and inducing nontrivial topological phases (Hung *et al.*, 2016). A principal manifestation of such topological phases is the existence of edge states that support directional transport and are robust against disorder (Lu, Joannopoulos, and Soljacic, 2014, 2016). In the optical domain, topological edge states have been observed in a number of linear photonic systems (absent atoms) such as helical waveguides (Rechtsman *et al.*, 2013) and coupled resonator arrays (Hafezi *et al.*, 2013). Adding atoms potentially provides a route toward interacting quantum topological photonic systems.

B. Perspective: Multiphysics coupling

Overall, aligning atomic transition frequencies in PhC band gaps leads to coherent Hamiltonians of the general form $H_{\rm bg} \sim \hbar\sum_{jl} f(z_j, z_l)\sigma^j\sigma^l$, while highly suppressing the effects of unwanted dissipation mechanisms. The sum of possibilities encoded in $H_{\rm bg}$ is rich, going beyond the exploration of long-range interacting spin systems previously described. For example, the atomic positions may also be treated as dynamical variables, in which case $f(z_j, z_l)$ represents a mechanical potential, and $H_{\rm bg}$ a system where the interatomic forces depend on their spin correlations. The associated forces can be very large compared to typical external traps, since they are derived from the vacuum-Rabi splitting $g_{\rm JC}$ associated with photons confined to the nanoscale. Finally, these nanophotonic interfaces are also able to achieve efficient photon-atom coupling. PhCs then potentially enable one to broadly explore novel quantum systems where atomic internal states (spins), motion (phonons), and photons are all strongly and coherently coupled. With these new possibilities in mind, in the following two sections we discuss some ways in which this multiphysics coupling can manifest itself.

X. SPINS AND MOTION: SEMICLASSICAL AND QUANTUM SELF-ORGANIZATION

In this section, we describe how strongly correlated states of spin and motion arise when the positions of the atoms in the band-gap interaction Hamiltonian [e.g., Eq. (18)] are treated as dynamical variables rather than being fixed. This builds upon an already rich body of work investigating "self-organization" of atoms, where the interplay between the scattering of light, the forces exerted, and the atomic positions are treated self-consistently.

Early pioneering work on self-organization investigated the case of atoms in a high-finesse cavity (Domokos and Ritsch, 2002; Black, Chan, and Vuletic, 2003), where atoms are driven by an external pump field propagating orthogonally to the cavity axis. Qualitatively, the atoms preferentially scatter photons from the pump into the cavity mode. This in turn builds up a standing-wave intensity whose force pushes atoms toward the antinodes and further enhances the atom-cavity coupling. Surprisingly, the steady-state configuration is one in which a spontaneously broken symmetry emerges, as atoms will organize into every other antinode. The origin of this effect is that the external pump drives atoms with the same phase, and that the cavity emission from dipoles in every other antinode would constructively interfere, while emission from every antinode would destructively interfere. Self-organization is also possible in other configurations, such as in a cavity where the pump field itself forms a standing wave, resulting in a Dicke quantum phase transition (Baumann *et al.*, 2010), multimode cavities (Gopalakrishnan, Lev, and Goldbart, 2009), or in one-dimensional waveguides (Chang, Cirac, and Kimble, 2013).

In previously considered systems, the spin degree of freedom is treated only classically, with the coherence operator σ_{ge} being approximated as a number such that the response of atoms to light is formally identical to that of a classical oscillating dipole. This can be justified on a number of grounds, for example, if the atoms are only weakly driven such that they mostly remain in the ground state, or if dissipation is sufficiently strong that spin correlations cannot build up. However, by using PCWs with atomic transitions in the band gap, it is possible for coherent spin interactions to strongly dominate over dissipation. If the atomic positions are dynamical variables, it might then be possible that a quantum self-organization can emerge, in which the stable spatial patterns of atoms, and the forces "binding" these patterns together, are due to entanglement in the spins. This also represents a highly exotic situation compared to typical materials, where the energy scales of crystallization and spin physics are completely different.

A simple example of such an effect can already be seen with just two atoms. Here we will consider the Raman scheme discussed in Sec. IX.A.1, where the band-gap interactions are used to facilitate coherent interactions within a ground-state manifold. This is necessary as for typical atomic excited states, both the interaction strength and emission rates are much larger than frequencies associated with motion. Using the Raman scheme it becomes possible to tune the interaction strengths to become comparable to motional scales, while incoherent loss rates become substantially smaller.

In a generic PCW, the spatial dependence of the interaction for frequencies within the band gap is $f(z_j, z_l) = e^{-|z_j - z_l|/L}\cos kz_j \cos kz_l$, resulting from the combination of the standing-wave structure of the Bloch mode and an exponential envelope for the two-point Green's function. Supposing that the atoms can be treated as point particles for now, one can consider adding an external trapping potential $V_T = V_0\sum_j \sin^2 k_T z_j$, where $k_T = k/2$ is chosen for conceptual simplicity to trap atoms at every other node of the APCW interaction, as illustrated in Fig. 14(a). This nominally results in zero interaction energy if atoms were to remain at the nodes. However, for two atoms, the spin part of the interaction in Eq. (18), $\sigma_{sg}^{(1)}\sigma_{gs}^{(2)} + \text{H.c.}$, has extremal eigenvalues of ± 1 for the entangled triplet and singlet states $|\pm\rangle = (|sg\rangle \pm |gs\rangle)/\sqrt{2}$), respectively. Thus, the interaction

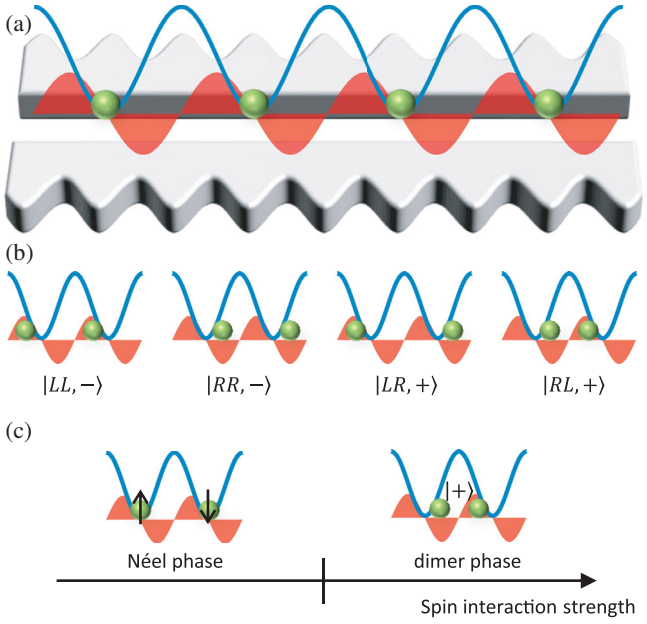

FIG. 14. (a) Trapping scheme to explore spin-motion coupling. The atoms (green) are trapped by an external potential (blue) at every second node of the Bloch function (red) of the PCW. (b) Considering a pair of atoms, interactions mediated by the photonic band gap lead the atoms to have lower energy if they displace from the nodes of the Bloch function (to the left $|L\rangle$ or right $|R\rangle$) and form either a spin triplet ($|+\rangle$) or singlet ($|-\rangle$). Without the exponential decay of the band-gap interactions the four possible configurations shown here would be degenerate. The exponential dependence of the band-gap interactions causes the state $|RL,+\rangle$ to be the lowest-energy configuration. (c) Many-body phase diagram. For weak band-gap interactions, the atomic wave packets are centered around the minimum of the external trapping potential, and the spins exhibit an antiferomagnetic Néel ordering. For larger interaction strengths, a spontaneously broken symmetry emerges where consecutive pairs of atoms form spatial dimers, while the internal spin state of the pair exhibits a large spin triplet fraction.

energy can always become negative, if each atom were to displace in one direction away from the nodes [left (L) or right (R)] and form an appropriate entangled state, as shown in Fig. 14(a). Without the exponential dependence of $f(z_j, z_l)$, four possible combinations would be degenerate in energy. However, the exponential most favors the two atoms becoming closer together in space, such that they form a spatial "dimer" $|RL\rangle$, which is associated with spin triplet $|+\rangle$. This effect is reminiscent of the spin-Peierls model (Peierls, 1955) in condensed matter physics, a simple one-dimensional model where a lattice instability arises due to spin-phonon coupling.

The interesting behavior seen at the level of two atoms naturally motivates an exploration of the many-body phase diagram, with one trapped atom per node. One limiting case, which was investigated analytically and numerically (Manzoni, Mathey, and Chang, 2017), consists of an interaction range L that is sufficiently small so that the nearest-neighbor approximation can be made. The motional degree of freedom is also treated quantum mechanically, projected into the two lowest bands of the external potential (for a deep lattice, the Wannier functions associated with these bands resemble the ground and first excited states of a harmonic oscillator potential, superpositions of which enable an atomic wave packet to be displaced to the left or right of the center of the trap).

The resulting phase diagram is qualitatively illustrated in Fig. 14(b). For sufficiently large band-gap interaction strength, the many-body ground state is gapped and undergoes a spontaneous symmetry breaking, with pairs of atoms forming spatial dimers, and the reduced two-atom density matrix exhibiting large overlap with the triplet $|+\rangle$ spin state (as might be anticipated from the two-atom example). Interestingly, for low interaction strength, the spins do not become noninteracting, as would be expected from classical point particles that sit exactly at the nodes of the PCW. Instead, the quantum zero-point motion enables spin interactions mediated by virtual excitation and annihilation of phonons and yields a ground state of antiferromagnetic or Néel spin ordering. Manzoni, Mathey, and Chang (2017) also considered the presence of an external magnetic field, which was found to yield additional exotic phases, including a gapped phase where atoms form spatial trimers accompanied by a fractional magnetization, and a "spin-motion fluid" phase where spin excitations and phonons form composite particles.

While the previous analysis focused on very specific parameter regimes, spin-motion coupling is expected to be an important effect in many settings. This is due to the combination of wavelength-scale spatial variations in the PCW-mediated interactions $f(z_j, z_l)$, and interaction strengths that can greatly exceed external trapping potentials, which yield strong spin-dependent forces. This mechanism has hardly been explored and should serve as a rich topic for future investigation.

XI. QUANTUM DIELECTRICS: PHOTON-PHOTON INTERACTIONS

We now discuss a different example of multiphysics coupling, wherein the band-gap-mediated spin interactions in a PCW can effectively result in interactions between propagating photons. A similar effect can already occur in light propagation through a Rydberg ensemble, as discussed in Sec. II, and which has produced beautiful demonstrations of highly nonlinear effects such as photon blockade. In that case, large nonlocal interactions between atoms excited to high-lying Rydberg levels map to strong interactions between the photons. In free space, the necessity to access high-lying Rydberg states is due to the combination of lifetime and interaction range that such states provide. PCWs offer a complementary approach, where by engineering the dispersion of light itself, even a normal atomic excited state has the required range of interactions and ratio of interaction strength to decay rate.

At first sight, band-gap-mediated interactions may not seem ideal for creating interactions between propagating photons as photons cannot propagate in a band gap. However, this problem is avoided by exploiting the multimode nature of realistic PCWs. For example, the APCW supports TM and TE modes as shown in Fig. 4(b), where the band gaps for the different modes occur over different frequency ranges. A

photon with frequency in the propagating band of the TM mode, and near resonant with an atomic transition frequency, can then be launched into the PCW and efficiently mapped into a spin excitation. This excitation can at the same time interact coherently via the band gap of the TE mode with other photon-spin polaritons. The novelty of this system can already be seen in the limit of infinite-range interactions as would be produced in conventional cavity QED. Such a system then effectively represents an atomic ensemble simultaneously coupled to a nanofiber (the TM mode) and cavity (the TE mode), which is a very difficult hybrid system to create in conventional settings.

By engineering the range and type of band-gap interaction as described in Sec. IX.A, the propagation of photons in the TM mode is affected in diverse ways. For example, in the case of two-level atoms with transition $|g\rangle$-$|e\rangle$ coupled resonantly to the probe, interactions of the form $\Sigma_{j\neq l} f(z_j, z_l)\sigma^j_{ee}\sigma^l_{ee}$ mean that excitation of atom j via the absorption of a single photon shifts the transition frequency of atoms l in the vicinity by an amount $f(z_j, z_l)$. Note that through the dependence of $f(z_j, z_l) \sim \cos kz_j \cos kz_l$ on the Bloch functions, atoms could be shifted in an alternating manner after the excitation of atom j, leading to an effective period doubling and a new effective band structure seen by subsequent photons (Albrecht, Caneva, and Chang, 2017). Alternatively, interactions of the form $\Sigma_{j\neq l} f(z_j, z_l)\sigma^j_{eg}\sigma^l_{ge}$ lead to anharmonicity in the excitation structure of the atomic ensemble, and for strong interactions the medium can act like a giant two-level system (Munro, Kwek, and Chang, 2017).

Before discussing a specific example in more detail, it is worthwhile to discuss techniques of solving for the dynamics of strongly interacting photons. Treating the propagating quantum field explicitly, and its interaction with atoms, represents an open, nonequilibrium quantum field theory, whose general solution is unknown. The spin model formalism described in Sec. V, specifically Eqs. (4)–(6), provides a promising alternative, through the realization that the field is not an independent degree of freedom [see Eq. (4)], but rather its properties are encoded in the dynamics of a finite (but possibly large) number of atomic spins evolving under Eqs. (5) and (6). Furthermore, reducing the problem to a system of spins potentially allows an extensive toolbox of condensed matter techniques to be applied to the photon propagation problem, where, for example, using matrix product states (Schollwock, 2011) one can access the dynamics of the many-body photon state (Manzoni, Chang, and Douglas, 2017).

For the case at hand, light propagation in a 1D waveguide with band-gap-mediated interactions can be modeled using a collection of spins evolving under the effective Hamiltonian $H_{\rm spin} = \tilde{H}_{\rm 1D} + H_{\rm atom} + H_{\rm pump} + H_{\rm bg}$. Here $\tilde{H}_{\rm 1D}$, given by Eq. (10), models the coupling of atoms to the TM mode, $H_{\rm bg}$ is the band-gap interaction, $H_{\rm atom}$ is the Hamiltonian of the bare atoms, and $H_{\rm pump}$ describes the coupling of the atoms to input light. Often in experiments the input probe light is a coherent state and this coupling can be described by

$$H_{\rm pump} = -\hbar\mathcal{E}_{\rm in}(t)\sqrt{\frac{\Gamma_{\rm 1D}}{2}}\sum_j(\sigma^j_{eg}e^{ik_pz_j} + \sigma^j_{ge}e^{-ik_pz_j})$$

for input pulse envelope $\mathcal{E}_{\rm in}(t)$ (Mollow, 1975). Once the spin dynamics are solved by evolving the system according to $H_{\rm spin}$ (along with the associated dissipative terms), the output field

$$\mathcal{E}_{\rm o}(z,t) = \mathcal{E}_{\rm in}(z,t) + \varepsilon_{\rm in}(z,t) + i\sqrt{\frac{\Gamma_{\rm 1D}}{2}}\sum_{j=1}^{N}\sigma^j_{ge}(t)e^{ik_p(z-z_j)}$$

is fully determined by the coherent input (classical part $\mathcal{E}_{\rm in}$ and vacuum fluctuations $\varepsilon_{\rm in}$) and the atomic coherence σ^j_{ge}. The calculation of output intensity $I = \langle\mathcal{E}^\dagger_{\rm o}\mathcal{E}_{\rm o}\rangle$ or higher order correlation functions such as $g^{(2)}$ then reduces to evaluation of atomic correlation functions.

In the spin model, the nature of $H_{\rm atom}$ is not constrained, and it can be used, for example, to study light propagation in ensembles of atoms in the EIT configuration discussed in Sec. II [see Fig. 2(d)]. In that figure, for atoms with three internal levels $|g\rangle$-$|e\rangle$-$|r\rangle$, EIT is modified by the presence of strong Rydberg interactions between the r levels. In the PCW case, instead of a Rydberg level, one uses a metastable state $|s\rangle$ as the third level [see the inset of Fig. 15(a)] and engineers a dispersive interaction similar to Rydberg states using a band gap $\Sigma_{j\neq l} f(z_j, z_l)\sigma^j_{ss}\sigma^l_{ss}$ (Douglas, Caneva, and Chang, 2016; Shahmoon *et al.*, 2016). Given the extra tunability of atom-atom interactions mediated by nanophotonic interfaces,

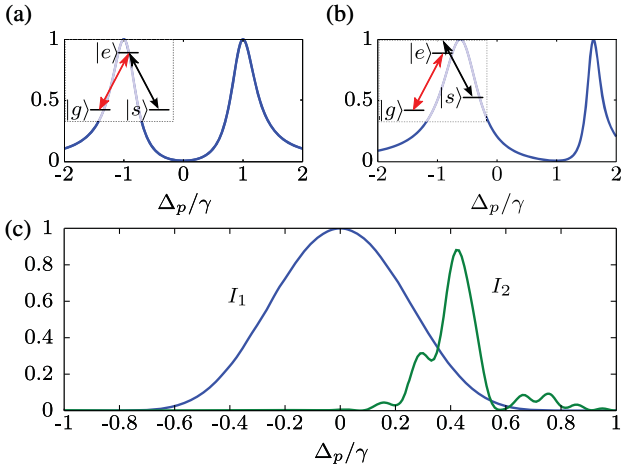

FIG. 15. (a) Imaginary part of the linear susceptibility (in arbitrary units) of an atom in the EIT configuration as a function of input probe detuning $\Delta_p = \omega_p - \omega_{eg}$. The imaginary part of the susceptibility is zero at zero detuning, indicating zero absorption of a continuous probe. Inset: The level structure of EIT, showing a probe field (red) on the $|g\rangle$-$|e\rangle$ transition and a control field on the $|s\rangle$-$|e\rangle$ transition. (b) A shift of the level s (inset) leads to a shifted atomic response where zero absorption is now achieved at a detuning $\Delta_p \neq 0$. (c) In a PCW, the shift of level s can occur via interactions with other atoms in level s. These interaction-induced shifts create new transparencies for different components of the input probe. Here we see the single-photon transmission I_1 is unaffected by the shift, while the two-photon transparency is shifted to the right as a result of uniform interactions $U = 0.5\Gamma$. Transmission is shown for an input coherent state and normalized by the input single-photon and two-photon intensities for control Rabi frequency $\Omega = 1.9\Gamma$ and an ensemble optical depth of 400.

combining them with EIT potentially allows for a more diverse range of nonlinear effects to be realized than with Rydberg atoms where the spatial dependence of the interaction is fixed by the Rydberg state.

The simplest example of a situation that cannot readily be achieved using (short-range) Rydberg interactions is a spatially uniform interaction across the atomic ensemble $f(z_j, z_l) = U$ (Caneva *et al.*, 2015; Douglas, Caneva, and Chang, 2016). In this case the transmission of single photons is unaffected by the interaction, where an individual photon entering the medium sees the normal EIT response of an atom shown in Fig. 15(a). In particular, perfect transparency results when the difference in frequencies between the probe and control fields matches the frequency difference between the states g and s. However, the presence of one polariton in the medium shifts the s levels of the atoms [Fig. 15(b)], and hence the EIT transparency condition for a second photon that enters. New EIT resonances then become available in the system, where two or more polaritons can propagate together if their combined detunings from the bare EIT resonance compensate for the shift resulting from the interaction. This behavior is shown in Fig. 15(c), where it is seen that the peak in the spectrum for the simulated transmitted intensity $I = \langle \mathcal{E}_o^\dagger \mathcal{E}_o \rangle$ of a weak continuous input field occurs at a different detuning than the peak in the two-photon "intensity" $I_2 = \langle \mathcal{E}_o^\dagger \mathcal{E}_o^\dagger \mathcal{E}_o \mathcal{E}_o \rangle$. More generally, for spatially dependent interactions these "correlated transparency windows" also depend on the position of the polartitons in the atomic ensemble. For example, by designing the interaction between the atoms to have a minimum at a finite atomic separation d, the two-photon transparent state takes the form of a photon molecule, where two photons propagate through the system separated by d (Douglas, Caneva, and Chang, 2016).

Going beyond a few photons, the many-body behavior of photons propagating in PCW systems is expected to display rich phenomena. A first step has been made in this direction, by a perturbative treatment that reveals weak crystal-like correlations in the many-body excitations of the photons (Shahmoon *et al.*, 2016). Developing a more general understanding of the dynamics of strongly interacting photons, in PCWs and in other platforms, is challenging and constitutes one of the exciting frontiers of quantum optics (Noh and Angelakis, 2017).

XII. OUTLOOK

In this Colloquium, we described some of the major new paradigms for controlling atom-light interactions within nanophotonic systems and their potential toward applications and realizing novel many-body phenomena. These possibilities are made possible by a combination of advances in nanophotonics design and fabrication, atomic trapping techniques, and theory of quantum light-matter interactions. A number of impressive proof-of-principle experiments already demonstrate the power of these interfaces. We have also tried to highlight the room for further technical and technological advances, which will help to turn the interface of atoms and nanophotonics into a mature field.

As an outlook, we speculate that ideas born within this field might also find impact in and infuse with other fields. For example, the possibility to realize chiral atom-light interactions (Mitsch *et al.*, 2014) already has stimulated investigations of many-body behavior in exotic chiral open systems (Lodahl *et al.*, 2017). The ability to tailor atom-light interactions using photonic crystals and dispersion engineering will likely be useful in other settings, such as "circuit QED" with superconducting qubits or in quantum optomechanical networks. In the case of circuit QED, for example, coupling of single qubits to waveguides (open transmission lines) can routinely reach ratios of $\Gamma_{1D}/\Gamma' \sim 10^2$ (van Loo *et al.*, 2013), and recently a single qubit has also been coupled to a microwave photonic crystal consisting of 14 unit cells (Liu and Houck, 2017). There has also been extensive work recently to realize topological effects in systems such as arrays of photonic resonators (Hafezi *et al.*, 2013) or of optomechanical elements defined in photonic crystals (Peano *et al.*, 2015). While these effects thus far are classical, adding atoms would be a natural way to bring such systems into the quantum regime.

An additional intriguing possibility is that the theoretical tools developed to treat atom-light interactions in complex dielectric environments (Sec. V) might find use in much more general settings. In particular, Eqs. (4) and (7) imply that atom-light interactions are formally encoded in the solution to an interacting open spin system. This in turn invites a separate set of techniques and insight, originating from the condensed matter community, to interpret atomic effects. For example, the dynamics of one-dimensional spin systems can be numerically simulated using matrix product states (Schollwock, 2011) providing a route toward near-exact solutions for photon propagation that go beyond previous perturbative or low-photon treatments (Sanchez-Burillo *et al.*, 2014; Manzoni, Chang, and Douglas, 2017). Separately, using this formalism, it has been shown that an ordered array of atoms (Barredo *et al.*, 2016; Endres *et al.*, 2016) in free space can *by itself* be a photonic crystal, supporting guided modes that do not spontaneously emit away energy (Zoubi and Ritsch, 2010; Sutherland and Robicheaux, 2016; Asenjo-Garcia, Moreno-Cardoner *et al.*, 2017; Shahmoon *et al.*, 2017). Taken together, this body of theoretical and experimental progress, and of potential connections to other fields, certainly points to an unexpected and much richer future for atoms and nanophotonics as compared to when efforts first began in this field.

ACKNOWLEDGMENTS

We thank our many colleagues who have contributed to the work described in this Colloquium, including Ignacio Cirac, Ana Asenjo-Garcia, Akihisa Goban, Alexey Gorshkov, Jonathan Hood, Mikhail Lukin, Marco Manzoni, Oskar Painter, Cindy Regal, Tao Shi, and Su-Peng Yu. A. G. T. acknowledges support from the Intra-European Marie-Curie Fellowship NanoQuIS (No. 625955) and the ERC grant QUENOCOBA, ERC-2016-ADG (Grant No. 742102). C. L. H. acknowledges support from the Air Force Office of Scientific Research (AFOSR) Young Investigator Program (No. FA9550-17-1-0298) and the Office of Naval Research (ONR) (No. N00014-17-1-2289). D. E. C. and J. S. D.

acknowledge support from Fundacio Privada Cellex, Spanish MINECO Severo Ochoa Program SEV-2015-0522, MINECO Plan Nacional Grant CANS and Explora Grant NANOTRAP, CERCA Programme/Generalitat de Catalunya, and ERC Starting Grant FOQAL. D. E. C. and H. J. K. acknowledge support from the AFOSR MURI Photonic Quantum Matter and the ONR MURI Quantum Opto-Mechanics with Atoms and Nanostructured Diamond (QOMAND). H. J. K. acknowledges funding from the ONR (No. N00014-16-1-2399), NSF Grant No. PHY-1205729, the Institute for Quantum Information and Matter (IQIM), and support as a Max Planck Distinguished Scholar that enabled his participation in this collaboration.

REFERENCES

Agarwal, G. S., 1975, Phys. Rev. A **12**, 1475.
Aidelsburger, M., M. Atala, M. Lohse, J. T. Barreiro, B. Paredes, and I. Bloch, 2013, Phys. Rev. Lett. **111**, 185301.
Akahane, Y., T. Asano, B.-S. Song, and S. Noda, 2005, Opt. Express **13**, 1202.
Albrecht, A., T. Caneva, and D. Chang, 2017, New J. Phys. **19**, 115002.
Albrecht, B., Y. Meng, C. Clausen, A. Dareau, P. Schneeweiss, and A. Rauschenbeutel, 2016, Phys. Rev. A **94**, 061401.
Andre, A., and M. Lukin, 2002, Phys. Rev. Lett. **89**, 143602.
Angelakis, D. G., M. F. Santos, and S. Bose, 2007, Phys. Rev. A **76**, 031805.
Aoki, T., B. Dayan, E. Wilcut, W. P. Bowen, A. S. Parkins, T. J. Kippenberg, K. J. Vahala, and H. J. Kimble, 2006, Nature (London) **443**, 671.
Araujo, M. O., I. Kresic, R. Kaiser, and W. Guerin, 2016, Phys. Rev. Lett. **117**, 073002.
Arcari, M., *et al.*, 2014, Phys. Rev. Lett. **113**, 093603.
Asano, T., B.-S. Song, and S. Noda, 2006, Opt. Express **14**, 1996.
Asenjo-Garcia, A., J. D. Hood, D. E. Chang, and H. J. Kimble, 2017, Phys. Rev. A **95**, 033818.
Asenjo-Garcia, A., M. Moreno-Cardoner, A. Albrecht, H. Kimble, and D. Chang, 2017, Phys. Rev. X **7**, 031024.
Badolato, A., K. Hennessy, M. Atature, J. Dreiser, E. Hu, P. M. Petroff, and A. Imamoglu, 2005, Science **308**, 1158.
Bajcsy, M., S. Hofferberth, V. Balic, T. Peyronel, M. Hafezi, A. S. Zibrov, V. Vuletic, and M. D. Lukin, 2009, Phys. Rev. Lett. **102**, 203902.
Bajcsy, M., A. S. Zibrov, and M. D. Lukin, 2003, Nature (London) **426**, 638.
Baragiola, B. Q., L. M. Norris, E. Montaño, P. G. Mickelson, P. S. Jessen, and I. H. Deutsch, 2014, Phys. Rev. A **89**, 033850.
Barclay, P. E., K. Srinivasan, O. Painter, B. Lev, and H. Mabuchi, 2006, Appl. Phys. Lett. **89**, 131108.
Barredo, D., S. de Leseleuc, V. Lienhard, T. Lahaye, and A. Browaeys, 2016, Science **354**, 1021.
Baumann, K., C. Guerlin, F. Brennecke, and T. Esslinger, 2010, Nature (London) **464**, 1301.
Bay, S., P. Lambropoulos, and K. Molmer, 1997, Phys. Rev. A **55**, 1485.
Beige, A., D. Braun, and P. L. Knight, 2000, New J. Phys. **2**, 22.
Beige, A., D. Braun, B. Tregenna, and P. L. Knight, 2000, Phys. Rev. Lett. **85**, 1762.
Bender, H., P. W. Courteille, C. Marzok, C. Zimmermann, and S. Slama, 2010, Phys. Rev. Lett. **104**, 083201.
Bermudez, A., T. Schaetz, and D. Porras, 2011, Phys. Rev. Lett. **107**, 150501.
Bhat, N. A. R., and J. E. Sipe, 2006, Phys. Rev. A **73**, 063808.
Bienias, P., S. Choi, O. Firstenberg, M. F. Maghrebi, M. Gullans, M. D. Lukin, A. V. Gorshkov, and H. P. Büchler, 2014, Phys. Rev. A **90**, 053804.
Birkl, G., M. Gatzke, I. Deutsch, S. Rolston, and W. D. Phillips, 1995, Phys. Rev. Lett. **75**, 2823.
Black, A. T., H. W. Chan, and V. Vuletic, 2003, Phys. Rev. Lett. **91**, 203001.
Brune, M., F. Schmidt-Kaler, A. Maali, J. Dreyer, E. Hagley, J. M. Raimond, and S. Haroche, 1996, Phys. Rev. Lett. **76**, 1800.
Buhmann, S. Y., and D.-G. Welsch, 2007, Prog. Quantum Electron. **31**, 51.
Caneva, T., M. T. Manzoni, T. Shi, J. S. Douglas, J. I. Cirac, and D. E. Chang, 2015, New J. Phys. **17**, 113001.
Carmichael, H. J., 1993, Phys. Rev. Lett. **70**, 2273.
Carusotto, I., and C. Ciuti, 2013, Rev. Mod. Phys. **85**, 299.
Casimir, H. B. G., and D. Polder, 1948, Phys. Rev. **73**, 360.
Cassagne, D., C. Jouanin, and D. Bertho, 1996, Phys. Rev. B **53**, 7134.
Chance, R. R., A. Prock, and R. Silbey, 2007, Adv. Chem. Phys. **37**, 1.
Chaneliere, T., D. N. Matsukevich, S. D. Jenkins, S.-Y. Lan, T. A. B. Kennedy, and A. Kuzmich, 2005, Nature (London) **438**, 833.
Chang, D. E., J. I. Cirac, and H. J. Kimble, 2013, Phys. Rev. Lett. **110**, 113606.
Chang, D. E., L. Jiang, A. V. Gorshkov, and H. J. Kimble, 2012, New J. Phys. **14**, 063003.
Chang, D. E., K. Sinha, J. M. Taylor, and H. J. Kimble, 2014, Nat. Commun. **5**, 4343.
Chang, D. E., A. S. Sorensen, E. A. Demler, and M. D. Lukin, 2007, Nat. Phys. **3**, 807.
Chang, D. E., V. Vuletic, and M. D. Lukin, 2014, Nat. Photonics **8**, 685.
Choi, K. S., H. Deng, J. Laurat, and H. J. Kimble, 2008, Nature (London) **452**, 67.
Chou, C.-W., J. Laurat, H. Deng, K. S. Choi, H. de Riedmatten, D. Felinto, and H. J. Kimble, 2007, Science **316**, 1316.
Clauser, J. F., 1974, Phys. Rev. D **9**, 853.
Colombe, Y., T. Steinmetz, G. Dubois, F. Linke, D. Hunger, and J. Reichel, 2007, Nature (London) **450**, 272.
Contreras-Reyes, A. M., R. Guerout, P. A. M. Neto, D. A. R. Dalvit, A. Lambrecht, and S. Reynaud, 2010, Phys. Rev. A **82**, 052517.
Corzo, N. V., B. Gouraud, A. Chandra, A. Goban, A. S. Sheremet, D. V. Kupriyanov, and J. Laurat, 2016, Phys. Rev. Lett. **117**, 133603.
Dalvit, D., P. Milonni, D. Roberts, and F. da Rosa, 2011, Eds., *Casimir Physics* (Springer, Berlin).
Darquie, B., M. P. A. Jones, J. Dingjan, J. Beugnon, S. Bergamini, Y. Sortais, G. Messin, A. Browaeys, and P. Grangier, 2005, Science **309**, 454.
Deutsch, I., R. Spreeuw, S. Rolston, and W. D. Phillips, 1995, Phys. Rev. A **52**, 1394.
de Vries, P., D. V. van Coevorden, and A. Lagendijk, 1998, Rev. Mod. Phys. **70**, 447.
Dicke, R. H., 1954, Phys. Rev. **93**, 99.
Domokos, P., and H. Ritsch, 2002, Phys. Rev. Lett. **89**, 253003.
Douglas, J. S., T. Caneva, and D. E. Chang, 2016, Phys. Rev. X **6**, 031017.
Douglas, J. S., H. Habibian, C.-L. Hung, A. V. Gorshkov, H. J. Kimble, and D. E. Chang, 2015, Nat. Photonics **9**, 326.
Dowling, J. P., and J. Gea-Banacloche, 1996, in *Advances In Atomic, Molecular, and Optical Physics*, Vol. 37, edited by B. B. a. H. Walther (Academic Press, New York), pp. 1–94.

Duan, L.-M., M. D. Lukin, J. I. Cirac, and P. Zoller, 2001, Nature (London) **414**, 413.

Duan, L.-M., and C. Monroe, 2008, in *Advances In Atomic, Molecular, and Optical Physics*, Vol. 55, edited by E. Arimondo, P. R. Berman, and C. C. Lin (Academic Press, New York), pp. 419–463.

Dudin, Y. O., and A. Kuzmich, 2012, Science **336**, 887.

Dung, H. T., L. Knoll, and D.-G. Welsch, 2002, Phys. Rev. A **66**, 063810.

Dzsotjan, D., A. S. Sorensen, and M. Fleischhauer, 2010, Phys. Rev. B **82**, 075427.

Endres, M., H. Bernien, A. Keesling, H. Levine, E. R. Anschuetz, A. Krajenbrink, C. Senko, V. Vuletic, M. Greiner, and M. D. Lukin, 2016, Science **354**, 1024.

Facchi, P., and S. Pascazio, 2002, Phys. Rev. Lett. **89**, 080401.

Faez, S., P. Türschmann, H. R. Haakh, S. Götzinger, and V. Sandoghdar, 2014, Phys. Rev. Lett. **113**, 213601.

Ficek, Z., and S. Swain, 2002, J. Mod. Opt. **49**, 3.

Ficek, Z., and R. Tanas, 2002, Phys. Rep. **372**, 369.

Firstenberg, O., C. S. Adams, and S. Hofferberth, 2016, J. Phys. B **49**, 152003.

Fitzpatrick, M., N. M. Sundaresan, A. C. Li, J. Koch, and A. A. Houck, 2017, Phys. Rev. X **7**, 011016.

Fleischhauer, M., A. Imamoglu, and J. P. Marangos, 2005, Rev. Mod. Phys. **77**, 633.

Fleischhauer, M., and M. D. Lukin, 2000, Phys. Rev. Lett. **84**, 5094.

Freedman, S. J., and J. F. Clauser, 1972, Phys. Rev. Lett. **28**, 938.

Friedrich, H., G. Jacoby, and C. G. Meister, 2002, Phys. Rev. A **65**, 032902.

Fushman, I., D. Englund, A. Faraon, N. Stoltz, P. Petroff, and J. Vuckovic, 2008, Science **320**, 769.

Garcia, P. D., S. Smolka, S. Stobbe, and P. Lodahl, 2010, Phys. Rev. B **82**, 165103.

Gardiner, C., and P. Zoller, 2004, *Quantum Noise* (Springer, New York).

Gardiner, C. W., 1993, Phys. Rev. Lett. **70**, 2269.

Gardiner, C. W., and M. J. Collett, 1985, Phys. Rev. A **31**, 3761.

Glauber, R. J., and M. Lewenstein, 1991, Phys. Rev. A **43**, 467.

Goban, A., K. S. Choi, D. J. Alton, D. Ding, C. Lacroute, M. Pototschnig, T. Thiele, N. P. Stern, and H. J. Kimble, 2012, Phys. Rev. Lett. **109**, 033603.

Goban, A., C.-L. Hung, J. Hood, S.-P. Yu, J. Muniz, O. Painter, and H. Kimble, 2015, Phys. Rev. Lett. **115**, 063601.

Goban, A., *et al.*, 2014, Nat. Commun. **5**, 3808.

Goldstein, E. V., and P. Meystre, 1997, Phys. Rev. A **56**, 5135.

Gong, Z.-X., M. Foss-Feig, S. Michalakis, and A. V. Gorshkov, 2014, Phys. Rev. Lett. **113**, 030602.

Gonzalez-Tudela, A., C.-L. Hung, D. E. Chang, J. I. Cirac, and H. J. Kimble, 2015, Nat. Photonics **9**, 320.

Gonzalez-Tudela, A., D. Martin-Cano, E. Moreno, L. Martin-Moreno, C. Tejedor, and F. J. Garcia-Vidal, 2011, Phys. Rev. Lett. **106**, 020501.

Gonzalez-Tudela, A., V. Paulisch, D. Chang, H. Kimble, and J. Cirac, 2015, Phys. Rev. Lett. **115**, 163603.

Gonzalez-Tudela, A., V. Paulisch, H. Kimble, and J. Cirac, 2017, Phys. Rev. Lett. **118**, 213601.

Gonzalez-Tudela, A., and D. Porras, 2013, Phys. Rev. Lett. **110**, 080502.

Gopalakrishnan, S., B. L. Lev, and P. M. Goldbart, 2009, Nat. Phys. **5**, 845.

Gorniaczyk, H., C. Tresp, J. Schmidt, H. Fedder, and S. Hofferberth, 2014, Phys. Rev. Lett. **113**, 053601.

Gouraud, B., D. Maxein, A. Nicolas, O. Morin, and J. Laurat, 2015, Phys. Rev. Lett. **114**, 180503.

Greentree, A. D., C. Tahan, J. H. Cole, and L. C. L. Hollenberg, 2006, Nat. Phys. **2**, 856.

Greiner, M., O. Mandel, T. Esslinger, T. W. Hansch, and I. Bloch, 2002, Nature (London) **415**, 39.

Grimm, R., M. Weidemuller, and Y. B. Ovchinnikov, 2000, in *Advances In Atomic, Molecular, and Optical Physics*, Vol. 42, edited by Benjamin Bederson and Herbert Walther (Academic Press, San Diego), pp. 95–170.

Gross, M., and S. Haroche, 1982, Phys. Rep. **93**, 301.

Gruner, T., and D.-G. Welsch, 1996, Phys. Rev. A **54**, 1661.

Grünzweig, T., A. Hilliard, M. McGovern, and M. Andersen, 2010, Nat. Phys. **6**, 951.

Hafezi, M., S. Mittal, J. Fan, A. Migdall, and J. M. Taylor, 2013, Nat. Photonics **7**, 1001.

Hammerer, K., A. S. Sørensen, and E. S. Polzik, 2010, Rev. Mod. Phys. **82**, 1041.

Haroche, S., and D. Kleppner, 1989, Phys. Today **42**, 24.

Haroche, S., and J.-M. Raimond, 2006, *Exploring the Quantum: Atoms, Cavities, and Photons* (Oxford University Press, Oxford).

Hartmann, M. J., F. G. S. L. Brandao, and M. B. Plenio, 2006, Nat. Phys. **2**, 849.

Hauke, P., and L. Tagliacozzo, 2013, Phys. Rev. Lett. **111**, 207202.

Hetet, G., L. Slodicka, M. Hennrich, and R. Blatt, 2011, Phys. Rev. Lett. **107**, 133002.

Hood, J. D., A. Goban, A. Asenjo-Garcia, M. Lu, S.-P. Yu, D. E. Chang, and H. J. Kimble, 2016, Proc. Natl. Acad. Sci. U.S.A. **113**, 10507.

Hung, C.-L., A. González-Tudela, J. I. Cirac, and H. J. Kimble, 2016, Proc. Natl. Acad. Sci. U.S.A. **113**, E4946.

Hung, C.-L., S. M. Meenehan, D. E. Chang, O. Painter, and H. J. Kimble, 2013, New J. Phys. **15**, 083026.

Hwang, J., M. Pototschnig, R. Lettow, G. Zumofen, A. Renn, S. Götzinger, and V. Sandoghdar, 2009, Nature (London) **460**, 76.

Jackson, J., 1999, *Classical Electrodynamics* (John Wiley & Sons, New York), 3rd ed.

Jaksch, D., and P. Zoller, 2003, New J. Phys. **5**, 56.

Jaynes, E., and F. Cummings, 1963, Proc. IEEE **51**, 89.

Joannopoulos, J. D., S. G. Johnson, J. N. Winn, and R. D. Meade, 2008, *Photonic Crystals: Molding the Flow of Light* (Princeton University Press, Princeton, NJ), 2nd ed.

John, S., and T. Quang, 1994, Phys. Rev. A **50**, 1764.

John, S., and T. Quang, 1996, Phys. Rev. Lett. **76**, 1320.

John, S., and J. Wang, 1990, Phys. Rev. Lett. **64**, 2418.

John, S., and J. Wang, 1991, Phys. Rev. B **43**, 12772.

Julsgaard, B., J. Sherson, J. I. Cirac, J. Fiurasek, and E. S. Polzik, 2004, Nature (London) **432**, 482.

Jurcevic, P., B. P. Lanyon, P. Hauke, C. Hempel, P. Zoller, R. Blatt, and C. F. Roos, 2014, Nature (London) **511**, 202.

Kato, S., and T. Aoki, 2015, Phys. Rev. Lett. **115**, 093603.

Kim, H., W. Lee, H.-G. Lee, H. Jo, Y. Song, and J. Ahn, 2016, Nat. Commun. **7**, 13317.

Kimble, H. J., M. Dagenais, and L. Mandel, 1977, Phys. Rev. Lett. **39**, 691.

Kimble, H. J., and L. Mandel, 1976, Phys. Rev. A **13**, 2123.

Klimov, V. V., and M. Ducloy, 2004, Phys. Rev. A **69**, 013812.

Knoll, L., S. Scheel, and D.-G. Welsch, 2000, in *Coherence and Statistics of Photons and Atoms*, edited by Jan Perina (Wiley, New York), pp. 1–64.

Kolovsky, A. R., 2011, Europhys. Lett. **93**, 20003.

Kurizki, G., 1990, Phys. Rev. A **42**, 2915.

Kuzmich, A., W. P. Bowen, A. D. Boozer, A. Boca, C. W. Chou, L.-M. Duan, and H. J. Kimble, 2003, Nature (London) **423**, 731.
Kuzmich, A., L. Mandel, and N. P. Bigelow, 2000, Phys. Rev. Lett. **85**, 1594.
Lalumiere, K., B. C. Sanders, A. F. van Loo, A. Fedorov, A. Wallraff, and A. Blais, 2013, Phys. Rev. A **88**, 043806.
Lambropoulos, P., G. M. Nikolopoulos, T. R. Nielsen, and S. Bay, 2000, Rep. Prog. Phys. **63**, 455.
Laucht, A., F. Hofbauer, N. Hauke, J. Angele, S. Stobbe, M. Kaniber, G. Bohm, P. Lodahl, M.-C. Amann, and J. J. Finley, 2009, New J. Phys. **11**, 023034.
Lehmberg, R., 1970, Phys. Rev. A **2**, 883.
Le Kien, F., V. I. Balykin, and K. Hakuta, 2004, Phys. Rev. A **70**, 063403.
Le Kien, F., S. Dutta Gupta, V. I. Balykin, and K. Hakuta, 2005, Phys. Rev. A **72**, 032509.
Le Kien, F., and A. Rauschenbeutel, 2014, Phys. Rev. A **90**, 063816.
Lester, B. J., N. Luick, A. M. Kaufman, C. M. Reynolds, and C. A. Regal, 2015, Phys. Rev. Lett. **115**, 073003.
Li, J., T. P. White, L. O'Faolain, A. Gomez-Iglesias, and T. F. Krauss, 2008, Opt. Express **16**, 6227.
Lidar, D. A., I. L. Chuang, and K. B. Whaley, 1998, Phys. Rev. Lett. **81**, 2594.
Lifshitz, E. M., 1956, Sov. Phys. JETP **2**, 73.
Lin, J., J. P. B. Mueller, Q. Wang, G. Yuan, N. Antoniou, X.-C. Yuan, and F. Capasso, 2013, Science **340**, 331.
Liu, C., Z. Dutton, C. H. Behroozi, and L. V. Hau, 2001, Nature (London) **409**, 490.
Liu, Y., and A. A. Houck, 2017, Nat. Phys. **13**, 48.
Lodahl, P., S. Mahmoodian, and S. Stobbe, 2015, Rev. Mod. Phys. **87**, 347.
Lodahl, P., S. Mahmoodian, S. Stobbe, A. Rauschenbeutel, P. Schneeweiss, J. Volz, H. Pichler, and P. Zoller, 2017, Nature (London) **541**, 473.
Lu, L., J. D. Joannopoulos, and M. Soljacic, 2014, Nat. Photonics **8**, 821.
Lu, L., J. D. Joannopoulos, and M. Soljacic, 2016, Nat. Phys. **12**, 626.
Lukin, M. D., M. Fleischhauer, R. Cote, L. M. Duan, D. Jaksch, J. I. Cirac, and P. Zoller, 2001, Phys. Rev. Lett. **87**, 037901.
Lund-Hansen, T., S. Stobbe, B. Julsgaard, H. Thyrrestrup, T. Sunner, M. Kamp, A. Forchel, and P. Lodahl, 2008, Phys. Rev. Lett. **101**, 113903.
Mabuchi, H., and H. J. Kimble, 1994, Opt. Lett. **19**, 749.
Manga Rao, V. S. C., and S. Hughes, 2007, Phys. Rev. B **75**, 205437.
Manzoni, M. T., D. E. Chang, and J. S. Douglas, 2017, Nat. Commun. **8**, 1743.
Manzoni, M. T., L. Mathey, and D. E. Chang, 2017, Nat. Commun. **8**, 14696.
Mazoyer, S., J. P. Hugonin, and P. Lalanne, 2009, Phys. Rev. Lett. **103**, 063903.
McCall, S. L., and E. L. Hahn, 1969, Phys. Rev. **183**, 457.
McCauley, A. P., A. W. Rodriguez, J. D. Joannopoulos, and S. G. Johnson, 2010, Phys. Rev. A **81**, 012119.
McGuirk, J. M., D. M. Harber, J. M. Obrecht, and E. A. Cornell, 2004, Phys. Rev. A **69**, 062905.
Miller, R., T. E. Northup, K. M. Birnbaum, A. Boca, A. D. Boozer, and H. J. Kimble, 2005, J. Phys. B **38**, S551.
Misra, B., and E. C. G. Sudarshan, 1977, J. Math. Phys. (N.Y.) **18**, 756.
Mitsch, R., C. Sayrin, B. Albrecht, P. Schneeweiss, and A. Rauschenbeutel, 2014, Nat. Commun. **5**, 5713.
Miyake, H., G. A. Siviloglou, C. J. Kennedy, W. C. Burton, and W. Ketterle, 2013, Phys. Rev. Lett. **111**, 185302.
Mollow, B. R., 1975, Phys. Rev. A **12**, 1919.
Muldoon, C., L. Brandt, J. Dong, D. Stuart, E. Brainis, M. Himsworth, and A. Kuhn, 2012, New J. Phys. **14**, 073051.
Munro, E., L. C. Kwek, and D. E. Chang, 2017, New J. Phys. **19**, 083018.
Murray, C., and T. Pohl, 2016, in *Advances In Atomic, Molecular, and Optical Physics*, edited by E. Arimondo, C. C. Lin, and S. F. Yelin (Academic Press, New York), Vol. 65, pp. 321–372.
Nayak, K. P., P. N. Melentiev, M. Morinaga, F. L. Kien, V. I. Balykin, and K. Hakuta, 2007, Opt. Express **15**, 5431.
Nogrette, F., H. Labuhn, S. Ravets, D. Barredo, L. Beguin, A. Vernier, T. Lahaye, and A. Browaeys, 2014, Phys. Rev. X **4**, 021034.
Noh, C., and D. G. Angelakis, 2017, Rep. Prog. Phys. **80**, 016401.
Notomi, M., K. Yamada, A. Shinya, J. Takahashi, C. Takahashi, and I. Yokohama, 2001, Phys. Rev. Lett. **87**, 253902.
O'Shea, D., C. Junge, J. Volz, and A. Rauschenbeutel, 2013, Phys. Rev. Lett. **111**, 193601.
Ovchinnikov, Y. B., S. V. Shul'ga, and V. I. Balykin, 1991, J. Phys. B **24**, 3173.
Painter, O., R. K. Lee, A. Scherer, A. Yariv, J. D. O'Brien, P. D. Dapkus, and I. Kim, 1999, Science **284**, 1819.
Patterson, M., S. Hughes, S. Combrie, N.-V.-Q. Tran, A. De Rossi, R. Gabet, and Y. Jaouen, 2009, Phys. Rev. Lett. **102**, 253903.
Paulisch, V., H. J. Kimble, and A. Gonzalez-Tudela, 2016, New J. Phys. **18**, 043041.
Peano, V., C. Brendel, M. Schmidt, and F. Marquardt, 2015, Phys. Rev. X **5**, 031011.
Peierls, R., 1955, *Quantum Theory of Solids* (Oxford University Press, New York).
Pelton, M., C. Santori, J. Vuckovic, B. Zhang, G. S. Solomon, J. Plant, and Y. Yamamoto, 2002, Phys. Rev. Lett. **89**, 233602.
Petersen, J., J. Volz, and A. Rauschenbeutel, 2014, Science **346**, 67.
Peyronel, T., O. Firstenberg, Q.-Y. Liang, S. Hofferberth, A. V. Gorshkov, T. Pohl, M. D. Lukin, and V. Vuletic, 2012, Nature (London) **488**, 57.
Phillips, D. F., A. Fleischhauer, A. Mair, R. L. Walsworth, and M. D. Lukin, 2001, Phys. Rev. Lett. **86**, 783.
Pichler, H., T. Ramos, A. J. Daley, and P. Zoller, 2015, Phys. Rev. A **91**, 042116.
Porras, D., and J. I. Cirac, 2008, Phys. Rev. A **78**, 053816.
Pritchard, J., K. Weatherill, and C. Adams, 2013, in *Annual Review of Cold Atoms and Molecules* (World Scientific, Singapore), Vol. 1, pp. 301–350.
Pritchard, J. D., D. Maxwell, A. Gauguet, K. J. Weatherill, M. P. A. Jones, and C. S. Adams, 2010, Phys. Rev. Lett. **105**, 193603.
Qi, X., B. Q. Baragiola, P. S. Jessen, and I. H. Deutsch, 2016, Phys. Rev. A **93**, 023817.
Ramos, T., H. Pichler, A. J. Daley, and P. Zoller, 2014, Phys. Rev. Lett. **113**, 237203.
Rechtsman, M. C., J. M. Zeuner, Y. Plotnik, Y. Lumer, D. Podolsky, F. Dreisow, S. Nolte, M. Segev, and A. Szameit, 2013, Nature (London) **496**, 196.
Reid, M. T. H., A. W. Rodriguez, J. White, and S. G. Johnson, 2009, Phys. Rev. Lett. **103**, 040401.
Reiserer, A., and G. Rempe, 2015, Rev. Mod. Phys. **87**, 1379.
Reitz, D., C. Sayrin, R. Mitsch, P. Schneeweiss, and A. Rauschenbeutel, 2013, Phys. Rev. Lett. **110**, 243603.
Rempe, G., H. Walther, and N. Klein, 1987, Phys. Rev. Lett. **58**, 353.
Richerme, P., Z.-X. Gong, A. Lee, C. Senko, J. Smith, M. Foss-Feig, S. Michalakis, A. V. Gorshkov, and C. Monroe, 2014, Nature (London) **511**, 198.

Ringel, M., M. Pletyukhov, and V. Gritsev, 2014, New J. Phys. **16**, 113030.
Ritter, R., N. Gruhler, W. Pernice, H. Kübler, T. Pfau, and R. Löw, 2015, Appl. Phys. Lett. **107**, 041101.
Ritter, R., N. Gruhler, W. H. P. Pernice, H. Kübler, T. Pfau, and R. Löw, 2016, New J. Phys. **18**, 103031.
Ritter, S., C. Nolleke, C. Hahn, A. Reiserer, A. Neuzner, M. Uphoff, M. Mucke, E. Figueroa, J. Bochmann, and G. Rempe, 2012, Nature (London) **484**, 195.
Rodriguez, A. W., A. P. McCauley, J. D. Joannopoulos, and S. G. Johnson, 2009, Phys. Rev. A **80**, 012115.
Rodriguez-Fortuno, F. J., G. Marino, P. Ginzburg, D. O'Connor, A. Martinez, G. A. Wurtz, and A. V. Zayats, 2013, Science **340**, 328.
Rosenberg, J., Q. Lin, and O. Painter, 2009, Nat. Photonics **3**, 478.
Safavi-Naeini, A. H., T. P. M. Alegre, J. Chan, M. Eichenfield, M. Winger, Q. Lin, J. T. Hill, D. E. Chang, and O. Painter, 2011, Nature (London) **472**, 69.
Saffman, M., T. G. Walker, and K. Mølmer, 2010, Rev. Mod. Phys. **82**, 2313.
Sames, C., H. Chibani, C. Hamsen, P. Altin, T. Wilk, and G. Rempe, 2014, Phys. Rev. Lett. **112**, 043601.
Sanchez-Burillo, E., D. Zueco, J. J. Garcia-Ripoll, and L. Martin-Moreno, 2014, Phys. Rev. Lett. **113**, 263604.
Sayrin, C., C. Clausen, B. Albrecht, P. Schneeweiss, and A. Rauschenbeutel, 2015, Optica **2**, 353.
Sayrin, C., C. Junge, R. Mitsch, B. Albrecht, D. O'Shea, P. Schneeweiss, J. Volz, and A. Rauschenbeutel, 2015, Phys. Rev. X **5**, 041036.
Schachenmayer, J., B. P. Lanyon, C. F. Roos, and A. J. Daley, 2013, Phys. Rev. X **3**, 031015.
Schilke, A., C. Zimmermann, P. W. Courteille, and W. Guerin, 2011, Phys. Rev. Lett. **106**, 223903.
Schlosser, N., G. Reymond, I. Protsenko, and P. Grangier, 2001, Nature (London) **411**, 1024.
Schollwock, U., 2011, Ann. Phys. (Amsterdam) **326**, 96.
Sekoguchi, H., Y. Takahashi, T. Asano, and S. Noda, 2014, Opt. Express **22**, 916.
Shahmoon, E., P. Grisins, H. P. Stimming, I. Mazets, and G. Kurizki, 2016, Optica **3**, 725.
Shahmoon, E., and G. Kurizki, 2013, Phys. Rev. A **87**, 033831.
Shahmoon, E., D. S. Wild, M. D. Lukin, and S. F. Yelin, 2017, Phys. Rev. Lett. **118**, 113601.
Shen, J. T., and S. Fan, 2005, Opt. Lett. **30**, 2001.
Shimizu, F., 2001, Phys. Rev. Lett. **86**, 987.
Shomroni, I., S. Rosenblum, Y. Lovsky, O. Bechler, G. Guendelman, and B. Dayan, 2014, Science **345**, 903.
Short, R., and L. Mandel, 1983, Phys. Rev. Lett. **51**, 384.
Solano, P., J. A. Grover, J. E. Hoffman, S. Ravets, F. K. Fatemi, L. A. Orozco, and S. L. Rolston, 2017, in *Advances in Atomic, Molecular, and Optical Physics*, edited by E. Arimondo, C. C. Lin, and S. F. Yelin (Academic Press, New York), Vol. 66, pp. 439–505.
Sollner, I., *et al.*, 2015, Nat. Nanotechnol. **10**, 775.
Søndergaard, T., and B. Tromborg, 2001, Phys. Rev. A **64**, 033812.
Sorensen, H., J.-B. Beguin, K. Kluge, I. Iakoupov, A. Sorensen, J. Muller, E. Polzik, and J. Appel, 2016, Phys. Rev. Lett. **117**, 133604.
Srinivasan, K., and O. Painter, 2002, Opt. Express **10**, 670.
Stannigel, K., P. Rabl, and P. Zoller, 2012, New J. Phys. **14**, 063014.
Stern, N. P., D. J. Alton, and H. J. Kimble, 2011, New J. Phys. **13**, 085004.
Sullivan, D., 2013, *Electromagnetic simulation using the FDTD method* (John Wiley & Sons, New York).
Sutherland, R. T., and F. Robicheaux, 2016, Phys. Rev. A **94**, 013847.
Swingle, B., G. Bentsen, M. Schleier-Smith, and P. Hayden, 2016, Phys. Rev. A **94**, 040302.
Takayama, S.-i., H. Kitagawa, Y. Tanaka, T. Asano, and S. Noda, 2005, Appl. Phys. Lett. **87**, 061107.
Tanji-Suzuki, H., I. D. Leroux, M. H. Schleier-Smith, M. Cetina, A. T. Grier, J. Simon, and V. Vuletić, 2011, Adv. At. Mol. Opt. Phys. **60**, 201.
Tey, M. K., Z. Chen, S. A. Aljunid, B. Chng, F. Huber, G. Maslennikov, and C. Kurtsiefer, 2008, Nat. Phys. **4**, 924.
Thompson, J. D., T. G. Tiecke, N. P. de Leon, J. Feist, A. V. Akimov, M. Gullans, A. S. Zibrov, V. Vuletic, and M. D. Lukin, 2013, Science **340**, 1202.
Thompson, R. J., G. Rempe, and H. J. Kimble, 1992, Phys. Rev. Lett. **68**, 1132.
Tiarks, D., S. Baur, K. Schneider, S. Durr, and G. Rempe, 2014, Phys. Rev. Lett. **113**, 053602.
Tiecke, T. G., J. D. Thompson, N. P. de Leon, L. R. Liu, V. Vuletic, and M. D. Lukin, 2014, Nature (London) **508**, 241.
Topolancik, J., B. Ilic, and F. Vollmer, 2007, Phys. Rev. Lett. **99**, 253901.
van Enk, S. J., and H. J. Kimble, 2001, Phys. Rev. A **63**, 023809.
van Loo, A. F., A. Fedorov, K. Lalumiere, B. C. Sanders, A. Blais, and A. Wallraff, 2013, Science **342**, 1494.
Vernooy, D. W., A. Furusawa, N. P. Georgiades, V. S. Ilchenko, and H. J. Kimble, 1998, Phys. Rev. A **57**, R2293.
Vetsch, E., D. Reitz, G. Sague, R. Schmidt, S. T. Dawkins, and A. Rauschenbeutel, 2010, Phys. Rev. Lett. **104**, 203603.
Vlasov, Y. A., M. O'Boyle, H. F. Hamann, and S. J. McNab, 2005, Nature (London) **438**, 65.
Volz, J., R. Gehr, G. Dubois, J. Esteve, and J. Reichel, 2011, Nature (London) **475**, 210.
Wang, R., X.-H. Wang, B.-Y. Gu, and G.-Z. Yang, 2001, J. Appl. Phys. **90**, 4307.
Wasilewski, W., K. Jensen, H. Krauter, J. J. Renema, M. V. Balabas, and E. S. Polzik, 2010, Phys. Rev. Lett. **104**, 133601.
Wong, C. W., P. T. Rakich, S. G. Johnson, M. Qi, H. I. Smith, E. P. Ippen, L. C. Kimerling, Y. Jeon, G. Barbastathis, and S.-G. Kim, 2004, Appl. Phys. Lett. **84**, 1242.
Woods, L., D. Dalvit, A. Tkatchenko, P. Rodriguez-Lopez, A. Rodriguez, and R. Podgornik, 2016, Rev. Mod. Phys. **88**, 045003.
Wubs, M., L. G. Suttorp, and A. Lagendijk, 2004, Phys. Rev. A **70**, 053823.
Yao, P., V. Manga Rao, and S. Hughes, 2010, Laser Photonics Rev. **4**, 499.
Ye, J., H. J. Kimble, and H. Katori, 2008, Science **320**, 1734.
Yoshie, T., A. Scherer, J. Hendrickson, G. Khitrova, H. M. Gibbs, G. Rupper, C. Ell, O. B. Shchekin, and D. G. Deppe, 2004, Nature (London) **432**, 200.
Zanardi, P., and M. Rasetti, 1997, Phys. Rev. Lett. **79**, 3306.
Zang, X., *et al.* 2016, Phys. Rev. Applied **5**, 024003.
Zeuthen, E., M. J. Gullans, M. F. Maghrebi, and A. V. Gorshkov 2017, Phys. Rev. Lett. **119**, 043602.
Zoubi, H., and H. Ritsch 2010, Europhys. Lett. **90**, 23001.